second moment spectrum (the power absorption coefficient) by as much as about 10 frequency decades. The decalin solvent which supports the dichloromethane molecules in their supercooled environment undergoes a transition at a well-defined temperature[1] into a glass, and below this glass transition temperature the splitting of the peak of the very broad zero-order spectral moment disappears. As the temperature of the glassy solution is lowered further the zero moment peak becomes very broad, and becomes separated from the second moment peak in the far infrared by as much as fourteen decades of frequency. The peaks at low frequency are known as the α and β processes, and that in the far infrared γ process, recognized in 1980.[107,108] Clearly, any attempt to explain this development must involve molecular dynamical evolution from picoseconds to years. The zero-moment peak shifts into regions of very low frequency as this cooling process is continued. The peak of the second moment spectrum, the far infrared γ process, shifts upwards in frequency[1,107,108] as the environment in which the dichloromethane molecules librate becomes more and more constricted in the glass at low temperature. This constricting effect is counterbalanced by loss of energy (temperature) but is dominant in the far infrared. This is true generally, the zero- and second-order spectral moments move in opposite directions with temperature in a molecular liquid, above and below the normal melting point in supercooled solutions. This pattern of behaviour can be reproduced qualitatively by the itinerant oscillator, but with the lavish use of empiricism.[1] The diffusion theory available at the time of writing cannot describe, even qualitatively, the α, β, and γ processes and their frequency dependence as a function of temperature and pressure.

I. The Challenge to Computer Simulation

There have been many attempts at investigating the glass transition with computer simulation, but none has been completely successful in representing the multidecade spectral profile. The original, constant volume, algorithms of computer simulation[91] have been successful in many areas, but are not capable of producing phase changes in general. There have been some limited successes with rotator phase to liquid transitions, but the onset of crystallization is not well described by contemporary simulation algorithms. The importance of combined dielectric and far infrared spectroscopy is clear therefore. Even the most powerful contemporary theories and computer simulation algorithms are faced with the challenge of describing self-consistently the first few spectral moments obtained from observation of a simple asymmetric top such as dichloromethane, as it is gradually condensed from gas to liquid and supercooled in solution. Accurate data from these experimental techniques assume key importance when

it is realized that even the most advanced contemporary diffusion theory, such as the itinerant oscillator, fails at the fourth moment, and that most contemporary simulation algorithms fail at the fourth or sixth. It follows that it is critically important to study a specimen of molecular liquid such as dichloromethane whose high-frequency power absorption is clearly defined and free of interference from higher frequency infrared vibrational modes. It is possible to construct the fourth, and even the sixth, spectral moments of dichloromethane[86–90] bcause of its clean far infrared spectrum.

A combination of dielectric and far infrared data is a critical and continuing challenge to contemporary theories of molecular diffusion, and has made the most important advances in challenging the traditional approach. Other key experiments have also played a significant role in the advances of the last 20 years, and will be described as follows with reference to the same test liquid, dichloromethane, typical[1,4] of the largest class by far of molecular symmetries, the asymmetric top.

J. Survey of Data for Liquid Dichloromethane

A detailed survey[1] has provided the following picture of investigations into molecular dynamics using many of the available experimental techniques.

1. There is a great deal of data, but not well coordinated. These have been produced using far infrared absorption, acoustic dispersion, and nuclear magnetic resonance relaxation, with a smaller amount of Raman scattering from the molecular liquid.
2. The thermodynamic properties of the molecular liquid at equilibrium are fairly well known, but there is a critical gap when dealing with virial coefficients. There are few data on pressure second and third virial coefficients, and no dielectric virial coefficients.[24]
3. Partly because of this insufficient data base, in particular virial coefficients,[24] the intermolecular potential is not well defined. The existing descriptions are built up empirically, from the Lennard–Jones parameters,[12] for example, and have had limited success in describing experimental data sensitive to the pair potential. There have been no attempts so far to build up the dichloromethane pair potential from first, quantum mechanical, principles. The computer power and basis sets for such a calculation are however available, following the examples set recently for liquid water.[109–112]
4. There is a smaller amount of work available using modern techniques of light scattering, including Brillouin and Rayleigh scat-

tering, and techniques such as coherent anti-Stokes Raman and inverse Raman scattering.

5. There are a few Kerr effect studies,[24] the polarizability of the molecule is known, but its anisotropy less accurately. Some computations are available of the effective charges on the atoms of the dichloromethane molecule from quantum mechanical first principles.
6. There is usually no investigation of the role of pressure in these spectroscopic and thermodynamic observations, although high pressure spectral techniques are well developed.
7. Overall there is a pronounced lack of coordination and interlaboratory cooperation in the study of this simple asymmetric top. Contemporary progress can be made, however, with ingenuity in the face of sparse data.

K. The Relaxation of Nuclear Magnetic Resonance

The archives on nuclear magnetic resonance run into millions of printed pages.[113] However, the conclusions reached with this technique about molecular dynamics are still equivocal.

The physical process of interest is the relaxation of nuclear magnetic resonance, caused by magnetic interactions between nuclei of molecules which are diffusing in a liquid or other environment. Different isotopes or nuclei carried by a diffusing molecule have different resonance frequencies, and this can be used experimentally[113,114] to obtain information that is not available in dielectric–far infrared spectroscopy. This is the anisotropy of the molecular diffusion process, expressed as correlation times[1,4] of different orientation axes in the same molecule. A restriction of NMR relaxation techniques in general is that they can provide only correlation times, not the full time dependence of the correlation function. Frequencies involved in NMR relaxation are relatively low, compared with THz of the far infrared.

In the past 20 years several different types of NMR relaxation have been utilized for the study of anisotropy in molecular diffusion, and the results expressed as different types of correlation time.

1. The longitudinal, or spin-lattice, relaxation time can be measured in a simple ensemble of molecules containing nuclei with a single spin 1/2 placed in an external magnetic field.
2. The transverse, or spin–spin, relaxation time is measured perpendicular to the applied magnetic field. As for the spin–spin relaxation time, it measures the rate of decay of magnetization.
3. A number of NMR relaxation mechanisms can be used to probe molecular dynamics. Among these are nuclear magnetic dipole–dipole and dipole–quadrupole interactions among nuclei on the same or different molecules, techniques which depend intricately on the details of the molecular diffusion process, both intra- and intermolecular. They can be used to examine diffusion in molecules which carry the interacting nuclei. A third example is spin rotation interaction, which is due to the fact that a moving charge produces a magnetic field, causing the atomic nuclei of molecules in certain rotational states to experience additional magnetic fields. The spin rotation correlation time involves both the molecule's reorientational motion and the change in molecular angular momentum due to torques exerted by other molecules. It is therefore almost uniquely useful to produce information from the angular momentum and orientational correlation function simultaneously.

4. Other relaxation mechanisms such as those involved in the anisotropic chemical shift and technical advances such as nuclear Overhauser enhancement and Fouricr transform NMR spectroscopy can also be used to provide information about the overall molecular diffusion process.

In proton relaxation, dipole–dipole interaction usually dominates is molecular liquids, but quadrupole relaxation is overwhelmingly dominant in the relaxation of molecular nuclei with spins greater than 1/2, such as ^{13}C and ^{15}N. In other circumstances, appreciable contributions may result from other mechanisms cited above.

The results from several different studies of this nature have been reviewed for dichloromethane liquid[114] and compared with complementary data from the far infrared and microwave. Brier and Perry[114] found that the relaxation times from different literature sources were at variance with each other but there was enough consistency to show that rotational diffusion could not describe the data. For example, the spin lattice relaxation time was not a third of the dielectric relaxation time, as expected from Debye's inertialess theory of rotational diffusion (Section I).

The opportunity does exist in NMR relaxation to look at different nuclear resonance phenomena. If this is done over a range of temperature and pressure the anisotropy of the molecular diffusion process can be defined. A recent review[4] details the available evidence in this context and summarizes quantitatively with the help of computer simulation of dichloromethane.

L. The Challenge to the Theory of NMR Relaxation

The challenge becomes clear when data from NMR relaxation are used with those from other sources,[24] such as the far infrared, dielectric region, and Kerr effect relaxation. Such a combination,[4,114] used with computer simulation, shows that the traditional approach of (Section I) is unable to match the data quantitatively. The NMR relaxation data are often complicated and difficult to reduce to the form needed for comparison with theory.[114] Despite this and other drawbacks, NMR relaxation is uniquely capable of giving correlation times on the anisotropy of the molecular diffusion process if experimental coordination is achieved among laboratories.

M. Anisotropy of Diffusion in the Asymmetric Top

The nature of this challenge requires a proper description of the theory of anisotropic molecular diffusion in three dimensions in an asymmetric top. Section I has described the rotational diffusion theory for the spherical top, or alternativcly in the simplified case of a diffuser in a plane. In both cases the nonlinear Euler cross terms disappear and the mathematics become tractable. If the data indicate however that the diffusion is anisotropic, a more complicated theoretical structure is needed, based on the Euler–Langevin equations[1–4]

$$I_x\dot{\omega}_x - (I_y - I_z)\omega_y\omega_z = -I_x\beta_x\omega_x + I_x\dot{W}_x \tag{68}$$

$$I_y\dot{\omega}_y - (I_z - I_x)\omega_z\omega_x = -I_y\beta_y\omega_y + I_y\dot{W}_y \tag{69}$$

$$I_z\dot{\omega}_z - (I_x - I_y)\omega_x\omega_y = -I_z\beta_z\omega_z + I_z\dot{W}_z \tag{70}$$

which are written in frame (x, y, z) of the principal molecular moments of inertia I_i. Here ω_i are the molecular angular velocity components in this frame and β_i are three empirical friction coefficients. Unless there are available three independent data sources, they are not separately definable. The mathematical structure of these equations is complicated, and the solutions, even though approximate, are even more so,[1,4] suffering from the following drawbacks.

1. As for all rotational diffusion theories, the data from the dielectric and far infrared regions are not describable quantitatively.[1,5,12]
2. They always involve the three unknown friction coefficients.
3. They suffer from all the drawbacks of Debye type theory as described in Chapter I.

Without considerable theoretical modification and additional experimental information, properly coordinated, the evidence for anisotropic diffusion from NMR relaxation must remain qualitative in nature. On the other hand computer simulation can be used directly to provide anisotropic correlation times in dichloromethane.[4]

N. Light Scattering

The elements of the theory of light scattering[46] have been known since the turn of the century through the work of Rayleigh and his contemporaries. In recent years, lasers have brought greater precision to these investigations, especially to those of the depolarised component of light scattered from a liquid.

The scattering of light at right angles is often reported, using VV, VH, HV, and HH configurations, where V stands for vertical and H for horizontal scattered or incident light. These configurations describe changes in the polarization of the scattered light, due to the fact that when electromagnetic radiation is incident on a diffusing molecule it induces the dipole moment

$$\boldsymbol{\mu}(t) = \boldsymbol{\alpha}(t) \cdot \mathbf{n}_0 \cdot \boldsymbol{\epsilon}_0 \tag{71}$$

where $\mathbf{n}_0$ is the polarization vector of the applied field and $\boldsymbol{\epsilon}_0$ is the electric field strength. The tensor $\boldsymbol{\alpha}$ is the molecular polarizability. Equation (71) is written in the linear approximation, as the intensity of the laser is increased higher-order scattering effects become observable through higher-order polarizability tensors.[24] The polarizability can be split into two parts, one is determined by the molecular framework and its point-group symmetry, and the other by the distortions introduced by the bond vibrations within the molecule. The first component gives rise to polarized Rayleigh–Brillouin scattering, which is essentially due to fluctuations in density, and also to a depolarised component dependent on the orientational behavior of the individual molecules as they diffuse and scatter light. The vibration dependent parts are responsible for Raman scattering. Molecular diffusion processes contribute[46] to all four types of scattering in one way or another, and spectra from light scattering contain information on molecular dynamics. Depolarized Rayleigh scattering occurs at THz frequencies, and provides by Fourier transformation the second Legendre polynomial

$$C_{2R}(t) = \tfrac{1}{2}\langle 3(\mathbf{u}(t) \cdot \mathbf{u}(0))^2 - 1\rangle \tag{72}$$

which involves the orientational acf in the ideal self dynamic limit when all intermolecular cross correlations are ignored. Depolarized Rayleigh

scattering contains the same kind of information as that found in far infrared bandshapes, except that the latter is a first-order effect.[1] Theories of molecular diffusion should therefore be capable of describing both types of spectra consistently. Essentially speaking, if the intensity of the depolarized Rayleigh spectrum $[I(\omega)]$ is multiplied by ω^2 the result is very similar in frequency dependence to the far infrared power absorption under the same conditions. The Fourier transform of

$$M_2(\omega) = \omega^2 I(\omega) \tag{73}$$

is the second time derivative of $C_{2R}(t)$.

Both the depolarized Rayleigh spectrum and far infrared absorption contain information about acf's, intermolecular orientational ccf's, and the numerous[47–57] cross correlations between rotational and translational diffusion. The spectra complement each other and should ideally be used in combination in any investigation. Rotational diffusion produces the result[5] that the orientational correlation time from Rayleigh scattering should be three times shorter than that from the first rank equivalent (the first Legendre polynomial).[46] If this is not the case experimentally, then diffusion theory must be modified.

Polarized, Rayleigh–Brillouin, scattering is due to fluctuations in the positions of the diffusing molecules, and is a means of investigating translational processes superimposed on orientational motions. It is an essentially cooperative process, and is described theoretically in terms of the hydrodynamic concept[46] of fluctuation density. The many cross correlations between rotational and translational molecular motion (Section I) contribute to both polarized and depolarized light scattering. Rayleigh–Brillouin scattering involves the creation and destruction of phonons (sound waves), and is the high-frequency adjunct of sound dispersion.[46] This is roughly analogous to the way in which far infrared absorption is the high-frequency adjunct of dielectric relaxation and dispersion. It is observed in VV polarization, but is influenced only indirectly by the motions of individual molecules.[115–120] Depolarized Rayleigh scattering depends in contrast on the reorientation of individual molecules and is observed in VH or HV geometry. In the same way that far infrared spectroscopy and dielectric relaxation should be used to complement each other, so should ultra and hyper sound dispersion and light scattering. A more thorough investigation would also utilize other techniques such as NMR relaxation.

Using the test molecule dichloromethane, it is possible to review the extent to which contemporary investigators have achieved this aim of thoroughly probing the molecular dynamics of one liquid with complementary techniques.[1,4] This review reveals an imbalance of effort. There are

many investigations on the hyper and ultra acoustic properties, revealing a dispersion of sound in the GHz range, analogous to dielectric loss in the microwave frequency region. A few reports of Brillouin scattering have deduced hypersonic velocities in the liquid up to 7.2 GHz. There are far fewer measurements involving Rayleigh scattering reported in that review,[1,4] however, and these were carried out under inconsistent experimental conditions, thus blurring the overall picture.

O. Raman Scattering

The frequency shifts of Raman scattering are due essentially to differences in the energy of the molecule due to internal bond vibrations. The molecule absorbs radiation in one state and reemits the radiation in another, via the induced dipole moment. A Raman spectral feature is dependent on the derivative of the polarizability with respect to coordinate. The polarizability tensor of the diffusing molecule fluctuates as the molecule vibrates, and in general, vibrational Raman scattering is influenced by rotational diffusion. Any attempt to separate the two processes is approximate, and in some cases, meaningless. There are always cross correlations between vibration, rotation, and translation in a diffusing molecule which can be investigated with computer simulation but which are intractable with the traditional approach of Section I.

Depolarized Raman scattering is always the result of combined rotation and vibration, superimposed on translation of the molecule's diffusing centre of mass. Individual Raman features in a liquid are broadened by the molecular diffusion process. Depolarization is caused by the rotational motion of the diffusing molecule. If the scattered light is not depolarized, the correlation function is that of the vibrational mode at the frequency at which the light is scattered in VV geometry. The intensities of polarized and depolarized Raman spectra about the vibrational frequencies of interest can therefore be expressed essentially as the Fourier transforms

$$I_{VV}(\omega) \propto \int_{-\infty}^{\infty} \exp(i\omega t) C_{\text{vib}}(t)\, dt \tag{74}$$

$$I_{VH}(\omega) \propto \int_{-\infty}^{\infty} \exp(i\omega t) C_{\text{vib}}(t) C_{2R}(t)\, dt \tag{75}$$

where C_{vib} is the acf of the vibrational dynamics of the mode of scattering under consideration. As the molecule rotates, the polarizability tensor varies with time, giving rise to a rotational band, a broadening centered on the vibrational frequency of each proper mode in the spectrum. Rotational

broadening effects predominate for small molecules dissolved in inert solvents and vibrational broadening effects predominate in heavy polyatomic molecules or in the presence of hydrogen bonding. If it is assumed that the rotational and vibrational effects are not cross correlated, that is, that C_{2R} is statistically independent of C_{vib}, then the complete Raman spectrum of a dipolar molecule in the liquid state can be used to obtain information about the nature of molecular diffusion. For each peak in the spectrum the polarized Raman component provides the vibrational correlation function by careful Fourier transformation, and the depolarized spectrum provides according to Eq. (75) a convolution of the rotational and vibrational correlation functions.

A review[1] of seventeen reports on the test liquid dichloromethane revealed information on the Raman and hyper-Raman spectroscopy of the molecular liquid carried out under different experimental conditions. There was no clear indication[121,122] whether the vibration and rotation were accounted for accurately, that is, whether cross correlation was considered or discarded, but there were reported careful corrections for the internal field effect, the amplitude increase in the intensity of scattered radiation caused by differences in the field incident locally on the diffusing molecule, and the original intensity of the incoming laser beam.

There was, however, little attempt at coordinating the results with those from other techniques. Only a few of the available Raman bands had been utilized in these papers.

P. The Challenge to the Traditional Approach to Light Scattering

There are several different ways in which a combination of Rayleigh and Raman scattering can challenge the original theories of rotational diffusion and the itinerant oscillator. Correlation times can be compared from both techniques[4] and with the equivalents from computer simulation. The one from depolarized Rayleigh scattering was 1.85 ps, and equivalents from dielectric relaxation ranged from 0.5 ps in dilute solution to 1.45 ps in the pure liquid. The one from Rayleigh scattering is not three times shorter than that from dielectric relaxation in the pure liquid, as required by the traditional approach. Various other factors contribute which are absent in the theory of rotational diffusion and in related single molecule theories (those which deal with acf's of orientation).

1. Depolarized Rayleigh scattering contains information about statistical cross correlation of the molecular dynamics of one molecule with its diffusing neighbors. In this case the ccf takes the form

$$C_{2Rc}(t) = \frac{1}{2}\left\langle 3\sum_{i,j}\mathbf{u}_i(t)\cdot\mathbf{u}_j(0) - 1\right\rangle \tag{76}$$

which reduces at $t = 0$ to the second-order Kirkwood factor

$$K_{2Rc} = \frac{3}{2}\left\langle\sum_{i,j}\mathbf{u}_i\cdot\mathbf{u}_j\right\rangle - \frac{1}{2} \tag{77}$$

In general these cross correlations can be accounted for by implementation of Mori theory.[1]

2. Rayleigh–Brillouin scattering poses the problem of rotation–translation coupling.[46–57] This is imperfectly understood with conventional diffusion theory.

3. Raman scattering involves the cross correlation of intramolecular vibration and molecular rotation, and contemporary computer simulations[123–125] are addressing themselves to this problem through the appropriate ccf in the laboratory frame (X, Y, Z) and the moving frame (x, y, z).

Q. Neutron Scattering[126]

Neutrons are scattered from molecular liquids following the same fundamental equations as light (photon) radiation. The neutron has a finite mass and transfers momentum to the diffusing molecule in an inelastic collision. Wave particle duality applies to the neutron[126] and the equivalent wavelength is in the far infrared range in conventional scattering experiments with neutrons. Relatively low-energy neutrons ("cold" neutrons) are scattered inelastically from molecular liquids. The scattering of laser radiation, on the other hand, is elastic. The hydrogen atom is about as massive as the neutron, and has a large scattering cross section. Neutrons also possess spin,[126] and this adds an extra dimension to the theory of inelastic neutron scattering. The scattered neutron wave contains a coherent and incoherent portion, containing information respectively on individual molecular diffusion and on collective dynamical evolution. This information can be obtained separately for hydrogen-containing molecules because the nucleus of the hydrogen atom has a large spin incoherent cross section. Incoherent, inelastic, neutron scattering provides information on molecular diffusion.

However, there are no selection rules which limit the number of Legendre polynomials which can contribute to the scattering process through the relevant time-correlation functions of orientation. The theory of neutron scattering involves a weighted sum of spherical harmonics of all orders.

This sum is obtainable theoretically[114] only in very simple cases, from the inertialess Debye theory or from the equation (65) of free rotation.

The challenge of neutron-scattering data can be met properly only with computer simulation, which provides a consistent analysis for all the contributing spherical harmonics, and cross refers to other types of data. For the test liquid dichloromethane there has been a thorough analysis by Brier and Perry[114] of the incoherent inelastic neutron scattering spectrum at four scattering angles. The results were compared with NMR data from several sources. The data were sufficient to show up the limitations in the few simple theories considered by Brier and Perry. Neutron scattering would be more incisive, however, if used consistently with far infrared absorption and dielectric relaxation, for example, because neutron scattering data is low in resolution with large instrument corrections. New reactor designs are needed for progress, and this is more expensive than all other techniques put together.

R. Infrared Absorption

Infrared studies of molecular diffusion can be summarized symbolically through the Fourier transform

$$IR(\omega) \propto \int_{-\infty}^{\infty} \exp(i\omega t) C_{\text{vib}}(t) C_{IR}(t)\, dt \tag{78}$$

between the spectrum and the vibrational and rotational acf's. The orientational acf is[1,4] $\langle \mathbf{u}(t) \cdot \mathbf{u}(0) \rangle$ and is assumed to be unaffected by intermolecular correlations in the customary approach. If this assumption is accepted the broadening of the infrared spectrum would be a unique measure of the orientational dynamics of a liquid. However, this is almost never the case in practice, because of statistical crosscorrelation with vibration which cannot be deconvoluted as in Raman scattering, by switching from polarized to unpolarized spectra. Infrared bands are also affected in general by isotopes, Coriolis coupling, and vibrationally excited states (hot bands).

Nevertheless, the information in infrared absorption bands is clean enough to be a significant challenge in its own right to simple diffusion theory. In dichloromethane, for example, the nine fundamental vibrational modes can be used to define the anisotropy of molecular diffusion. The nature of rotational diffusion about each axis of the frame (x, y, z) can be observed in priniple[4] with an appropriate fundamental and the way it has been broadened about its peak frequency. It is assumed that the vibrational acf C_{vib} can be obtained from Raman scattering, but

in dichloromethane, this is available only for the totally symmetric vibrational mode. The required information from the Raman is not easily extracted because the Raman band shapes are not related straightforwardly to the reorientation of the symmetry axes of frame (x, y, z). Therefore, despite having available infrared active vibrations parallel to all three axes of frame (x, y, z), the lack of data on vibrational relaxation is a severe constraint. This can however be remedied with contemporary simulation algorithms.

In the 70 or so papers reviewed in Ref. 1 there are many attempts to factorize the vibrational and rotational correlation functions which ignore the cross correlation between these modes. The result is a conflict of conclusions with other sources such as NMR relaxation.[114] There are also discrepancies of up to 50% between results in different papers on the same dynamical process (e.g., diffusion of the dipole axis) using sources from the infrared and NMR relaxation. This limits the usefulness of the data until greater coordination is forged.

S. The Role of Computer Simulation in Data Coordination

Computer simulation is essentially a numerical method[91] of solving the classical equations of motion for a small number of diffusing molecules, typically in the range from 100 to 1000. Depending on the numerical approximations used in integrating the equations of motion, a number of useful time ccf's can be constructed directly from the numerical data by running time averaging. Their Fourier transforms are spectra of various kinds. Both spectra and correlation functions can be used to match consistently experimental data from all sources. This reduces everything to knowledge of the intermolecular pair potential, which can be computed ab initio. Simulation can, in principle, remove empiricism from the interpretation of liquid-state spectra.

T. Dielectric Relaxation and Far Infrared Absorption

The relevant time correlations are respectively the orientational

$$C_{\text{cross}} = \left\langle \sum_i \sum_j \mathbf{u}_i(t) \cdot \mathbf{u}_j(0) \right\rangle \tag{79}$$

of the diffusing dipole moment axis of one molecule and all the others in the ensemble; and its far infrared adjunct,[1] the rotational velocity correlation function, its second time derivative. As with all theories of dielectric relaxation,[9–15] the computation of these time correlation functions involves consideration of intermolecular correlations, as well as cross corre-

lations[46–57] between different dynamical quantities (such as angular and linear velocity) for one particular molecule of the ensemble. The observable spectrum of the molecular liquid presents itself in terms of statistical correlations of orientation vectors, the molecular dipole moments, but a complete understanding of the background dynamics is essential for a proper description of the spectrum. In this respect, computer simulation can contribute in many different ways, despite the fact that it is limited by its inherent numerical approximations to a description of the second spectral moment or power absorption coefficient. In recent years progress has been rapid in the following directions.

1. In the early 1980s, the present author constructed[1–4,127–130] the far infrared power absorption coefficient of liquid dichloromethane from computer simulation of 108 molecules interacting with a model atom–atom representation of the pair potential.[4,12,24] The spectrum was constructed from the auto correlation function, an approximation which neglected intermolecular cross corrrelations because of lack of computer power. This can be improved by using more molecules and by computing the complete cross correlation using an ab initio calculation of the pair potential.[131–133] Not only did the far infrared spectrum from the simulation provide an acceptable representation of the data but the trajectories generated were also used to generate more information about the dynamics. This removed many of the uncertainties caused by empiricism in the customary approach, and showed the existence of many new cross correlations.

2. The anisotropy of diffusion in dichloromethane[1,2,4] was obtained from the relevant correlation functions constructed from fundamental dynamical trajectories. Correlation times for direct comparison with the NMR, Raman, infrared, and neutron-scattering data were obtained from the areas beneath the correlation functions. This is impossible with the Euler–Langevin equations (68) to (70) because the three friction coefficients have never been determined experimentally. This is a clear illustration of the advantage of computer simulation over the theories of Section I. None of these can be used easily without the introduction of ad hoc empiricism, either in the fundamental equations or in closing the continued fractions.

3. Computer simulation was also used to interpret the correlation times from light scattering.[4]

4. The trajectories generated in the same simulation could be used to probe deeply into the nature of statistical ccf's in frames (X, Y, Z) and (x, y, z). The latter were checked against group theory (Sections V, VII, and VIII), resulting in detailed agreement. A correlation function prohibited by symmetry disappeared also in the simulation, and conversely.

5. The very foundations of the traditional approach were carefully investigated using ccf's in frame (X, Y, Z) and strong externally applied electric fields. The present author showed the existence[134–140] of several ccf's in frame (X, Y, Z) which the customary theories had missed. Several more appeared in response to an applied field such as an electric field. These new ccf's show that molecular diffusion is a much more intricate process than allowed for in the theories of Section I. The ccf's can be built up in computer simulation from the same set of trajectories as those used in the construction of observable spectra. Recent work (Sections VII and VIII) has shown that some of the new ccf's themselves explain fundamental observable phenomena. All this is completely outside the scope of a simple theory of rotational diffusion, however heavily parameterized. The vast majority of the new ccf's signal combined dynamics of rotation and translation, upon which vibration is superimposed. Some of the new ccf's appear only in frame (x, y, z)[141–144] or in frame (X, Y, Z) only in the presence of fields, vanishing at equilibrium. This strikes at the very roots of conventional methods used to describe a spectrum generated in the presence of an external field. This includes the technique of dielectric spectroscopy, which relies on conventional fluctuation–dissipation theory, assuming implicitly that the field generates no new ccf's of its own. This is discussed in greater depth and detail later in this chapter, but it is already apparent from this brief surface scratching exercise that the intensive and detailed work of the 1980s has altered the landscape of diffusion beyond recognition by a combination of key data and computer simulation.

III. COMPUTER SIMULATION

If a diffusing molecule is considered to be a rigid body that simultaneously rotates and translates in three dimensions through an ensemble of similar molecules, then it is assumed in this chapter that the trajectories can be described adequately with classical mechanics. The experimental consequences of this assumption will reveal the limit of its validity.

The numerical technique of computer simulation,[91] introduced in the 1950s and 1960s, solves the classical equations of motion for a small number of molecules, usually in the region from 100 to 1000. The original technique is based on the Newton equation of motion, adapted for rotational dynamics. Newton's equation can be summarised[145] as

$$m\ddot{\mathbf{r}}_i = \mathbf{F}_i = -\sum_j \frac{\partial \phi_{ij}}{\partial \mathbf{r}_i} \tag{80}$$

where m is the molecular mass, $\mathbf{F}_i$ the net force on a molecule i at the instant t, and $\mathbf{r}_i$ the position of the molecular centre of mass in frame (X, Y, Z) of the laboratory observer. Here ϕ_{ij} is the intermolecular pair potential, that between molecule i and j at time t. This equation is dependent on the intermolecular energy ϕ_{ij}. In the simple translational and rotational Langevin equations of Section I the intermolecular potential energy is represented in the first approximation by the friction coefficient in combination with the random force or torque, as the case may be. Langevin's equation is a Newton equation written as

$$m\ddot{\mathbf{r}}_i = -m\beta_T \dot{\mathbf{r}}_i + \mathbf{F}_i(\text{random}) \tag{81}$$

The intermolecular potential has been approximated in a particularly simple way. In one sense, the whole of the theory of molecular diffusion comes down to approximating the intermolecular potential energy generated by the diffusing molecule. The total potential energy $\Phi(\mathbf{r})$ generated by N such diffusing molecules (N is of the order of the Avogadro Number) can be written[145] as the series expansion

$$\Phi(\mathbf{r}) = \frac{1}{2!}\sum \phi_{ij}^2(\mathbf{r}_i, \mathbf{r}_j) + \frac{1}{3!}\sum \phi_{ijk}^3(\mathbf{r}_i, \mathbf{r}_j, \mathbf{r}_k) + \cdots \tag{82}$$

in terms of pair, three-body, four-body and n-body interactions. In an ideal gas of atoms, such as dilute gaseous argon, the higher-order terms can be neglected, and the complete potential energy can be approximated by the first term in the sum, the pair potential. For atomic argon this has customarily been approximated by the Lennard–Jones potential

$$\phi_{ij}(\mathbf{r}_i, \mathbf{r}_j) = 4\epsilon\left[\left(\frac{\sigma}{r_{ij}}\right)^{12} - \left(\frac{\sigma}{r_{ij}}\right)^{6}\right] \tag{83}$$

where ϵ and σ are adjustable but not purely empirical, because they originate partly in the theory of quantum mechanics.[146] The inverse sixth power comes from the London dispersion energy[146] which has no classical equivalent. This has a negative sign because it is an attractive term, whereas the electronic repulsion between two argon atoms is represented by the empirical inverse twelfth power of the interatomic distance.

In contemporary molecular dynamics computer simulation the pair potential between two molecules is often assumed to be a sum of Lennard–Jones pair potentials for each atom of the two molecules. This is known as the atom–atom Lennard–Jones representation of the pair potential

$$\phi_{ij}^{(12)}(\text{molecule}) = \sum_1 \sum_2 \phi_{ij}^{(12)}(\text{atom}) \tag{84}$$

This is a sum over all the possible atom–atom pair potentials that occur in molecules 1 and 2. If, for example, the molecules are simple diatomics of the type A–B then there are four atom–atom terms: A–A, B–B, A–B, and B–A. The terms A–A and B–B are the same as their equivalents in the isolated atoms A and B, but the cross terms A–B and B–A must be represented by the Lorentz–Berthelot combining rules

$$\sigma_{AB} = \tfrac{1}{2}(\sigma_A + \sigma_B); \qquad \epsilon_{AB} = (\epsilon_A \epsilon_B)^{1/2} \tag{85}$$

All these assumptions about the nature of the potential energy in an ensemble of diffusing molecules, that it can be represented as a sum of pair potentials between molecules, and that this can in turn be built up from a sum of atom–atom Lennard–Jones potentials, can be justified only by the results, and how they compare with experimental data. The use of the Lennard–Jones approximation, devised in the 1920s in response to the dramatic changes wrought by quantum mechanics, comes from the fact that there is still an inadequate contemporary knowledge of the true intermolecular potential energy. In the test molecule of Section II, dichloromethane, the experimental data[1,4] needed to define the intermolecular pair potential are sparse and inadequate (e.g., pressure and dielectric[24] virial coefficients). The basis sets and computer power for the direct computation of the pair potential ab initio now exist, but there seems to have been no exploration yet along these lines. This typifies the state of the art contemporarily. Furthermore, the whole of classical computer simulation exists only because there are no practical ways, yet, of solving the quantum mechanical equations of motion of an ensemble of diffusing molecules.

Progress can be made against these disadvantages by assuming that the atom–atom pair potential is transferable between molecules to some extent, that is, the quantity A–A in the representation of the intermolecular pair potential between molecule A–B and molecule A–B is about the same as that in any other molecule containing the atom A or B. On this basis, tables of atom–atom Lennard–Jones parameters have been drawn up[101–103] for many of the elements. These literature values are not purely

empirical, but are often based on fitting the atom–atom Lennard–Jones form to relevant experimental data, for example, gaseous viscosity,[147] thermal conductivity[148] and, where available, pressure second and third virial coefficients,[1] dielectric second virials,[24] and data such as those on crystal structure.[149] As a rule, the assessment of the dynamical (and spectral) results of a computer simulation should be tempered by the realization that they are obtained with a representation of the true intermolecular potential which may or may not have been adequately tested over a broad enough range of data from all available sources. The survey carried out in 1982 by the present author[1] found that the atom–atom Lennard–Jones potential for dichloromethane could be constructed from data on carbon, chlorine, and hydrogen, the three atomic components of the intermolecular potential, but that there was a serious lack of experimental information with which to assess the potential with any degree of accuracy. In another example, that of the water-water pair potential, a recent survey by Morse and Rice[111,112] using the crystalline structure of the numerous phases of ice found that no potential representation was adequate to reproduce the details available. The most successful water pair potential was not one based on the Lennard–Jones form at all, but from an ab initio computation[150] parameterised for use in a classical simulation algorithm.[151] This method is soundly based, but recquires a large investment of computer time. If inadequate basis sets are used, there may be misleading results for the heavier atoms. However, the ab initio method is destined to replace the models based on Lennard–Jones's approximation.

The technique of molecular dynamics computer simulation, as it stands at present, is not therefore an experimental method. It is a numerical method of solving the classical equations of motion assuming that they can be applied to diffusing molecules over picosecond time scales and angstrom dimensions. The great advantage of the technique over the traditional methods of Chapter 1 include its applicability to three-dimensional diffusion of the asymmetric top, involving simultaneous translation and rotation. Increasingly, simulation methods can also be applied to the diffusion of molecules which are vibrating.[104,105] The quantum mechanical rules governing the various vibrational modes of the molecular framework can be adapted numerically for use in a simulation algorithm.

A. Summary of Numerical Approximations

The method of solving the Newton equation in a collection of, for example, 108 molecules, proceeds[145] on the assumption that the complete potential energy generated by the interaction of any one molecule with all the others can be represented by the sum of $N(N-1)/2$ pair potentials, where N is the number of molecules in the ensemble. The force between any two atoms of two neighbouring and diffusing is approximated by the Lennard–Jones form, as is the contemporary practice in many cases. The complete intermolecular force is the sum of these atom–atom terms. The number of molecules must be restricted in the simulation because of the finite speed and capacity of the computer. This introduces at least two problems.

1. The range of the pair potential must be restricted or truncated at a finite distance, outside of which there is assumed to be no force between the molecules. In other words, the atom–atom potential is truncated at a distance[145] $r_C \simeq 2.5\sigma$.
2. An atom of the diffusing molecule interacts with a finite number of other atoms on other molecules. These are inside the cut-off sphere of radius r_C. There is assumed to be no interaction outside this cut-off sphere.

These approximations are usually basic to any computer simulation algorithm, but the most difficult to accept is the necessity of using periodic boundary conditions.[91,145]

B. Periodic Boundary Conditions

The sample of 108 molecules, for example, dichloromethane molecules, used in the computer simulation has a finite volume, which is usually kept constant (constant volume computer simulation). The kinetic and potential energies of the sample fluctuate considerably in the liquid condition, although the total energy should be constant.[91] In order to preserve this constancy to within a fraction of a percent the 108-molecule sample must be kept from disintegrating by natural diffusion of molecules out of the original sample volume. This is achieved by holding the sample in a cell, usually a cube. If the trajectory of any molecule takes it outside a wall of the cell, periodic boundary conditions ensure that it is not lost from the sample. Usually, a coding device ensures that if the centre of mass moves outside the wall it reenters through the opposing wall with identical velocity. The coordinates of reentry are coded to be the negative of those at which the original centre of mass departed. Periodic boundary conditions can be represented by

$$\dot{\mathbf{r}}(out) = \dot{\mathbf{r}}(in): \qquad (x_i, y_i, z_i)\,(out) = (-x_i, -y_i, -z_i)\,(in) \tag{86}$$

The effect of equations (86), which apply automatically to any molecule which leaves the cube is to preserve the total energy as a constant. Transla-

tional momentum is also conserved, and periodic boundary conditions do not allow net linear flow in the sample.

Their use raises a number of objections, in that the liquid has no periodicity in reality. In practice, however, the molecular dynamics sample is made large enough to eliminate edge and surface effects from the computation of quantities of interest.[145] In particular, time acf's and ccf's do not usually suffer from the effects of imposed periodicity. Numerous simulations[1–4] with different numerical methods[105] for the integration of the classical equations of motion have reinforced this conclusion. Periodic boundary conditions do not conserve the sample's angular momentum, and in consequence, computer simulation has been used to investigate dielectric polarisation due to an applied electric field. Such simulations have already discovered fundamentally new ccf's[141,142] as described in Section II. After 60 years of sporadic development the analytical theory of diffusion failed to anticipate their existence, and is still not capable of describing their time dependence. This is a clear sign of the advantages of computer simulation. The numerous numerical approximations inherent in the technique do not sap its ability to produce original results.

C. Numerical Integration of the Equations of Motion

The essence of the method of computer simulation is to take advantage of the speed of contemporary digital computers to integrate numerically the equations of motion of the sample of molecules under consideration. There are many different ways[91,145] of achieving this objective, with ever-increasing efficiency. The problem is essentially the integration of ordinary differential equations of motion. In this context the nonlinearities of the Euler equations have caused the greatest difficulty due to inherent singularities, but these difficulties have bccn circumvented in several different ways, using quaternions,[91] or by methods which directly compute the net molecular torque. The latter is integrated numerically for the molecular angular momentum and angular velocity. Two of the most popular methods for the numerical integration of the translational equations are the Gear predictor–corrector algorithm[145] and the leapfrog algorithm.[91]

D. The Gear Predictor–Corrector

The algorithm uses a Taylor expansion[145] to compute the position of the molecular centre of mass, $\mathbf{r}$, at $t + \Delta t$ given its position at the initial instant t. The Taylor series can be written as

$$\mathbf{r}(t + \Delta t) = \sum_{k=0}^{m} \Delta^k \frac{d^k}{dt^k} \mathbf{r}(t) \tag{87}$$

and is truncated at order m. The differential equation to be solved is a function of the derivatives of the Taylor expansion to order m. This is the "predictor." The "corrector" uses the predicted positions and derivatives to compute the exact mth derivative at the instant $t + \Delta t$. The difference between the exact and predicted mth derivative is then used to correct the derivatives of all orders using a forward differencing scheme.[145] In order to implement this algorithm the forces on the center of mass of the diffusing molecule must be known from a computation of the net forces on each atom. These are computed directly from a knowledge of the interatomic distances between atoms of different molecules by differentiation of the atom–atom potential energy terms. This is implemented for all molecules within the cut-off sphere, and the "forces-loop" is the most time-consuming of the whole algorithm. The cut-off sphere is affected by the cell-code algorithm, which assumes that the pair potential can be neglected beyond the cut-off distance, and by the implementation of periodic boundary conditions.

Usually, the cell-code algorithm is based on the division of the complete cube into subcells, so that the length of one side of the cube is an integer multiple of the sub-cell length, which is not less than the cut-off distance. The molecules are then sorted into sub-cells before the forces loop is implemented, which has the effect of sorting out which molecules are in the nearest-neighboring cells before proceeding with the computation of the net atomic forces for each molecule in the sample. The forces loop is a double loop, because there are $N(N - 1)/2$ interactions. The outer has N steps and the inner $(N - 1)$. For each molecule pair there are several atom–atom terms, so that the use of the nearest-neighbour sub-cells (or "lists") is a great time saver. Parallel implementation[104] on IBM-based architectures shares out the forces loop among different array processors.

Periodic boundary conditions must be applied before the sub-cell code is used.[91,145]

E. The Leapfrog Algorithm

Also known as the Verlet algorithm, this is stable and easy to code and is used to integrate[91] both translational and rotational equations. It uses a Taylor expansion of the center of mass position of each molecule as if it were subjected to a constant net force in the brief time interval Δt. This approximation leads to equations (66) and (67) of Section II. Adding these gives

$$r(t + \Delta t) = r(t) + \delta r(t) \tag{88}$$

where

$$\delta r(t) = \delta r(t - \Delta t) + F(t)\frac{\Delta t^2}{m} \tag{89}$$

The terms $\delta r(t)$ and $\delta r(t - \Delta t)$ are the position increments. Calculus then leads to the velocity $\dot{r}(t)$ of the center of mass[91]

$$\dot{r}(t) = \frac{r(t + \Delta t) - r(t - \Delta t)}{2\Delta t} \tag{90}$$

$$= \frac{\delta r(t - \Delta t)}{\Delta t} + \frac{1}{2}\frac{F(t)\Delta t^2}{m} \tag{91}$$

It can be shown from a Taylor expansion of the velocity (v) backwards and forwards by the increment $\Delta t/2$ that

$$v^{n+1/2} = \frac{\delta r(t)}{\Delta t} \tag{92}$$

and

$$v^{n-1/2} = \frac{\delta t(t - \Delta t)}{\Delta t} \tag{93}$$

where $v^{n+1/2}$ and $v^{n-1/2}$ are the half-time step velocities. The force at time $t = n\Delta t$ is calculated from the coordinates at time $n\Delta(t)$. It is then used to update the position increment from time $(n-1)\,\Delta t$ to Δt. This new velocity is then used in turn to update the coordinates to time $(n+1)\Delta t$.

After the coordinates are updated periodic boundary conditions are applied to make sure that all the molecules are inside the cube. Verlet's algorithm is a type of trapezoidal rule numerical integration.

Despite its simplicity, it is more stable than the various orders of Gear algorithm[91] for many applications. Its disadvantages are exposed with spectral moment data, because there are usually no time derivatives of the force, that is, higher-order terms in the Taylor expansions (66) and (67). Higher-order Gear algorithms[145] implement the time derivative of force, and its derivative in turn, but these have a destabilizing effect[91] when using large time steps, probably because of excess fluctuations in the force field. Higher-order Gear algorithms, used with small time steps, can however be tested against spectral moment data. A successful example of the computation of higher-order time correlation functions is given in Ref. 95 for liquid nitrogen. This shows that higher-order time correlation

functions and associated spectral moments are much more intricate than allowed for by customary diffusion theory, even when using approximants of the Mori and Grigolini continued fractions.[1–4]

F. Integration of the Rotational Equations

Equations of motion written directly in the Euler angles contain singularities which make them unsuitable for numerical integration. This has led to the quaternion method[91] of representing rotational motion in three dimensions of the diffusing asymmetric top. The rotational equations of motion are expressed as

$$\frac{d\mathbf{J}}{dt} = \mathbf{Tq} \tag{94}$$

and

$$\frac{d\mathbf{q}}{dt} = \mathbf{Q} \tag{95}$$

where $\mathbf{J}$ is the molecular angular momentum and $\mathbf{Tq}$ the torque on the diffusing molecule at time t. Here Eq. (95) is written in four-dimensional quaternion notation, the matrix $\mathbf{Q}$ being defined as

$$\mathbf{Q} = \frac{1}{2}\begin{bmatrix} -\zeta & -\chi & \eta & \xi \\ \chi & -\zeta & -\xi & \eta \\ \xi & \eta & \chi & \zeta \\ -\eta & \xi & -\zeta & \chi \end{bmatrix} \tag{96}$$

The orientation of the asymmetric top is represented in three dimensions through the four-parameter quaternion

$$\mathbf{q} = (\xi, \eta, \zeta, \chi)^T \tag{97}$$

subject to the constraint

$$\xi^2 + \eta^2 + \zeta^2 + \chi^2 = 1 \tag{98}$$

G. Other Molecular Dynamics Simulation Algorithms

There are now available many different types of general and specialist molecular dynamics computer simulation algorithms.[91,145] A library of

codes and program descriptions is available from the Daresbury Laboratory of the U.K. Science and Engineering Research Council. The majority of these integrate the classical rotational and translational equations of motion for the asymmetric top molecule in three dimensions, considering this as a rigid body. Increasingly, code is available for flexible molecules, using a method based on the translational equations of motion of each atom of the molecules constrained by a classical representation of the bonds between them.[103,104] An example of time ccf's from this technique can be found in Ref. (104). Exploratory work is in progress in many dimensions, the utilization of higher-order algorithms,[91] such as the Toxvaerd method,[152] the development of algorithms for large molecules such as proteins,[153] the parallel implementation of code for supercomputers,[154] and the rapid development of non-equilibrium simulation.[145] Improvements are also being made in the use of periodic boundary conditions, new link-cell techniques, neighborhood lists, the computation of flow phenomena and hydrodynamic properties, the simulation of the effect of external fields,[155–160] and in many other directions. Volumes of the specialist literature,[161] are increasingly dedicated to new material phases such as the glassy state, and phase transitions. Simulations are also available for the compressed and dilute gas states.[162–166]

This activity has occurred in the last 20 years and has changed most areas of specialization out of recognition. As far as the subject of molecular dynamics is concerned, one of the first signs of the power of the new technique appeared in the computer simulation by Rahman of 864 argon atoms in 1964.

H. Rahman's Computer Simulation of Liquid Argon

The equations of the translational motion of the 864 atoms were integrated numerically to produce results in conflict with the traditional approach to diffusion theory outlined in Section I. For example, the translational Langevin equation (1) produces an exponential for the velocity acf

$$C_v(t) = \langle \mathbf{v}(t) \cdot \mathbf{v}(0) \rangle = \langle v^2 \rangle \exp(-t/\tau_v) \tag{99}$$

where τ_v is the linear velocity correlation time. This result had never been seriously questioned, and never adequately tested experimentally over short enough time scales until the results of this computer simulation appeared in 1964. The prediction of the approximately correct value of the Avogadro Number from consideration of Brownian motion masked the theory's inherent limits. There were no experimental techniques available with which to test the validity of the exponential decay of Eq. (99).

Progress towards such a test had been made slowly, but had resulted in no more than the Green–Kubo relation[167]

$$D_v = \frac{1}{3}\int_0^\infty \langle \mathbf{v}(t) \cdot \mathbf{v}(0) \rangle \, dt \tag{100}$$

between the diffusion coefficient and the acf. It had always been assumed by the vast majority that the time dependence itself was exponential. The simulation proved this to be a fallacy.

1. The time acf from the simulation became negative as t increased. It displayed a long negative tail.
2. The acf had a zero slope at $t = 0$, that is, was differentiable at zero time, unlike the simple exponential of the Langevin diffusion equation (1).

These results initiated a vast literature on the corrections necessary[1–4] to account for the numerical results. These attempts are still being made, using many different approaches. This is a clear indication that the simulation leads the theory towards new results.

I. Some Fundamental Properties of Time Correlation Functions

In order to understand more clearly the conflicts between the diffusion theory and the results produced numerically it is necessary to look at the Taylor expansion of the time correlation function, $C(t)$, of two arbitrary and stationary functions of time, $A(t)$ and $B(0)$. This is a real and statistically stationary[1] function of time for a dynamical variable such as linear velocity, implying

$$C_v(t) = \langle \mathbf{v}(t) \cdot \mathbf{v}(0) \rangle = \langle \mathbf{v}(-t) \cdot \mathbf{v}(0) \rangle = \langle \mathbf{v}(0) \cdot \mathbf{v}(-t) \rangle \tag{101}$$

Considering the Taylor expansion of this function it can be shown as follows that the odd time derivatives of the classical time correlation function vanish.

Consider the fundamental property

$$C_v(t) = \langle \mathbf{v}(t) \cdot \mathbf{v}(0) \rangle = \langle \mathbf{v}(t + \tau) \cdot \mathbf{v}(\tau) \rangle = \langle \mathbf{v}(t - \tau) \cdot \mathbf{v}(\tau) \rangle \tag{102}$$

of the statistically stationary time correlation function at reversible thermodynamic equilibrium. It follows that

$$\langle \dot{\mathbf{v}}(t+\tau)\cdot\mathbf{v}(\tau)\rangle = -\langle \dot{\mathbf{v}}(t-\tau)\cdot\mathbf{v}(\tau)\rangle \tag{103}$$

At $t = 0$ the following results are obtained:

$$\langle \dot{\mathbf{v}}(0)\cdot\mathbf{v}(0)\rangle = -\langle \mathbf{v}(t)\cdot\dot{\mathbf{v}}(0)\rangle \tag{104}$$

and

$$\langle \dot{\mathbf{v}}(0)\cdot\mathbf{v}(0)\rangle = 0 \tag{105}$$

Taking the second derivative,

$$\frac{d^2}{dt^2}\langle \mathbf{v}(t)\cdot\mathbf{v}(0)\rangle = -\langle \dot{\mathbf{v}}(t)\cdot\dot{\mathbf{v}}(0)\rangle \tag{106}$$

and continuing the process

$$\frac{d^{2n}}{dt^{2n}}\langle \mathbf{v}(t)\cdot\mathbf{v}(0)\rangle = (-1)^n\left\langle \frac{d^n}{dt^n}\mathbf{v}(t)\cdot\frac{d^n}{dt^n}\mathbf{v}(0)\right\rangle \tag{107}$$

The classical time acf is therefore an even function of time, with the Taylor expansion

$$C_\nu(t) = \langle \nu^2(0)\rangle - \frac{t^2}{2!}\langle \dot{\nu}^2(0)\rangle + \frac{t^4}{4!}\langle \ddot{\nu}^2(0)\rangle - \cdots \tag{108}$$

where Taylor coefficients $\langle \nu^{2n}(0)\rangle$ are spectral moments. The present author showed[44] that the memory functions of the Mori theory of diffusion must also be even functions of time, with well-defined Taylor coefficients related to those of the time correlation function from which the set of memory functions is derived.

At short times, therefore, the time acf of the linear velocity in Rahman's simulation must be

$$C_\nu(t) \simeq \langle \nu^2(0)\rangle - \frac{t^2}{2!}\langle \dot{\nu}^2(0)\rangle \tag{109}$$

that is, the slope at $t = 0$ is zero. The exponential acf from the Langevin equation (1) contravenes this general law because the slope of the exponential is finite and the mean square force $\langle \dot{\nu}^2\rangle$ is not definable. The exponential is not differentiable at $t = 0$.

J. The Long Time Tail

The most telling departure from the exponential is a long negative tail as $t \to \infty$. Intense research into its origin, using simulation and analytical theory, revealed the persistent correlation at long times, the long time tail, to be due to back-flow. The original translation of an atom sets up cooperative motion in neighbouring atoms. An analogy in hydrodynamics is that of spherical particle flowing through a continuous medium. In the same way that a ship marks its path in the water, a translating atom sets up statistically correlated motions of the centers of mass of neighbors which are themselves diffusing. Gradually, a pattern of correlation is built up, which affects the diffusion of the original atom itself. Further research in the wake of Rahman's pioneering work showed[168–172] that both the linear and angular acf's in simulations of molecular diffusion show a time dependence as $t \to \infty$, which is different from the exponential decay expected from the Langevin equations. Explanations of these long time tails were sought in theories[170–172] based on hydrodynamics applied at the molecular level. Some contemporary simulations, using as many as 200,000 atoms, have confirmed[173] that hydrodynamic phenomena, vortices, eddies, and flows, can be generated in a well-defined manner directly from Newton's equation applied to atoms. This closes the gap in our understanding of atomic and molecular phenomena and hydrodynamics, continuum concepts of flow, and provides confidence in the basic applicability and validity of computer simulation in many fields of chemical and theoretical physics and engineering. The traditional approach of Section I cannot explain the long time tails, with the possible exception of some approximants of the Grigolini continued fraction. These appear in several acf's, including the orientational, that of the rotational and angular velocities, as well as that of the linear velocity. Several lines of approximation in recent years have converged to show that when details of the environment (other diffusing molecules) are accounted for properly, using computer simulation, many new correlations appear in the description of the dynamics. A complete understanding of spectral data can be obtained only with computer simulation as a powerful guide to interpretation. This is not to denigrate the approach of Section I, which has provided an important evolutionary base, but one which can be built upon to great advantage.

K. The Interaction between Rotational and Translational Molecular Diffusion

The presence of long time tails has shown that the rotational and translational diffusion of molecules is statistically correlated in several ways. Once a diffusing molecule is given shape, and once we escape from the

confines of separated rotational diffusion, as proposed (with good reason) by Debye, these correlations must be taken into consideration. The theory of hydrodynamics is already richly endowed with concepts which spring from a combination of rotational and translational motions. An example is vortex flow set up downstream of an obstacle. By generalizing the concepts of hydrodynamics, and adapting them for an individual diffusing molecule, it can be shown that its angular velocity acf takes the asymptotic form[168,169,173]

$$C_\omega(t)(t \to \infty) = \frac{d\pi I}{2mn}(4\pi(D + \nu))^{-(d+2)/2} t^{-(d+2)/2} \tag{110}$$

where I, m, n, ν, and D are respectively the molecular moment of inertia, molecular mass, number density, kinematic shear viscosity, self-diffusion coefficient, and dimensionality of the system. For diffusion in two dimensions, $d = 2$, and in three dimensions, $d = 3$. It follows[1] from this relation that the orientational acf

$$\langle \mathbf{u}(t) \cdot \mathbf{u}(0) \rangle \propto \langle u^2(0) \rangle t^{-(d+2)/2} \tag{111}$$

that is, must behave asymptotically as $t^{-(d+2)/2}$. Double differentiation to produce the rotational velocity acf shows that

$$\langle \dot{\mathbf{u}}(t) \cdot \dot{\mathbf{u}}(0) \rangle \propto \langle \dot{u}^2(0) \rangle t^{-(2+(d+2)/2)} \tag{112}$$

By Fourier transformation of the relevant correlation functions (111) and (112) it follows that the low-frequency regions of the dielectric loss and the far infrared power absorption coefficient must contain information on the processes responsible for the long time tails. These spectra contain information on the kinematic shear viscosity, which appears in the relevant asymptotic expressions (110)–(112) for the time correlation functions of the diffusing molecule. This is well known in the theory of light scattering[46] as the "shear doublet" observed at low frequency. No description of the dielectric and far infrared spectral range can be complete without a proper description of the interrelation between rotation and translation. This is discussed in greater detail in Section V, using the new computer simulation results of the last 5 years, obtained for asymmetric tops diffusing in three dimensions. A complete general theory must be capable of generating all these results self consistently, and of interrelating molecular and hydrodynamic concepts.

L. Simulation of Liquid Dichloromethane

The simulation of an asymmetric top diffusing in three dimensions became possible in the early 1980s due to the work of several groups. Within the framework of the European Molecular Liquids Group and the CCP5 Committee of the U.K. Science and Engineering Research Council these algorithms are now freely available to individual scientists who wish to apply them. The emergence of this powerful new technique has meant that the spectral data available from several different sources could be tested numerically for consistency from a representation of the pair potential. This task was undertaken by the present author and co-workers and the results published[1–4] in several review articles for different molecules. For each molecule, the dynamics and available spectral data were probed numerically with an algorithm called TETRA, written by Schofield, Singer, Ferrario, and Evans, full details of which are in the literature.[174] This robust algorithm has now produced a wide variety of new results on several aspects of combined rotational and translational motion in the asymmetric top. This work has pervaded some 150 articles in the specialist literature. A listing and brief explanation of the code is provided in Appendix 1. Video animations of the molecular dynamics of several systems using this algorithm are also available from IBM, Kingston, New York, Dept. 48B/428, and from the author.

In the test liquid dichloromethane, the available experimental data from the sources described in Section II, and others, were tested for consistency with a model potential[175–180] from the atom–atom Lennard–Jones parameters in the literature for chlorine, hydrogen, and carbon. Using these three parameters, which can be refined experimentally, it is possible with TETRA to generate many types of information corresponding to the different spectra. Using the dynamical trajectories generated, during the simulations the variety of statistical ccf's produced by group theory (see Sections V, VII and VIII), in frames (x, y, z) and (X, Y, Z) could be computed entirely self-consistently. The algorithm therefore provides a link between a variety of spectral data and the emerging concepts of hydrodynamics adapted for the motion of individual molecules. The time step used in these computations was 5.0 fs (5.0×10^{-15} sec). This was sufficient to produce stability in the total energy to within $\pm 0.1\%$. A complete description of the results is available in several publications, conveniently collected in Refs. (2) and (4).

M. Comparison of Simulation with Spectral Data

The task of comparing thoroughly the range of available dynamical data on liquid dichloromethane with results from the computer simulation be-

gins with the definition of the intermolecular potential to be used in the simulation. For dichloromethane, with two relatively large chlorine atoms, there is as yet no really adequate ab initio computation of the pair potential as a function of intermolecular distances and relative molecular orientation. Such results are slowly becoming available and it is hoped that the necessary basis sets and methods will soon be used.

This is typical of contemporary knowledge on intermolecular potentials, even for small molecules. The alternative but more empirical Lennard–Jones atom–atom approximation is therefore implemented as a working alternative.

N. The Lennard–Jones Atom–Atom Potential for Dichloromethane

The literature on atom Lennard–Jones parameters usually provides them in the form ϵ/k and σ. For dichloromethane there are several literature sources which do not necessarily provide the same values for these parameters for each atom, in this case H, Cl, and C. This is an unsatisfactory contemporary state of affairs which can only be remedied partially by tuning the Lennard–Jones parameters to given experimental data. In the simulations carried out by Ferrario and Evans,[1,4] which formed the basis for the survey of the properties of dichloromethane, the parameters were taken from the literature but adjusted slightly to provide best agreement with the internal energy of the liquid as measured exprimentally and with the specific heat at constant volume. The Lennard–Jones parameters actually used were

$$\sigma(H-H) = 2.75A \qquad \epsilon/K(H-H) = 13.4\,K$$
$$\sigma(Cl-Cl) = 3.35\,A \qquad \epsilon/k(Cl-Cl) = 175.0\,K$$
$$\sigma(C-C) = 3.20\,A \qquad \epsilon/K(C-C) = 51.0\,K$$

and cross terms were evaluated with Lorentz–Berthelot combining rules.

The representation of the pair potential was completed with electrostatic terms, point charges on each atom. This is a first approximation to the electrostatic attraction between two dichloromethane molecules which does not take into account that the molecule is polarisable.[12,24] The point charges used in the potential were obtained from a quantum mechanical computation which represents the electron cloud of the molecule as fractional charges on each atom, a crude first approximation which continues to be unavoidable in classical approximations to the true quantum potential. The numerical fractional charges were $0.098|e|$ on H; $-0.109|e|$ on Cl; and $0.022|e|$ on C; $e = -1.6 \times 10^{-19}$ C.

O. Computer Simulation Methods

Having established the approximation to the pair potential, the aim of the computer simulation was to reproduce as accurately as possible as broad a range as possible of dynamical data obtained from observed spectra[1,4] of liquid dichloromethane, and its solutions in non-dipolar molecules such as carbon tetrachloride.

The constant volume algorithm TETRA was initiated by setting up the dichloromethane molecules on a lattice, for convenience a face-centred cubic lattice. The algorithm then generated the necessary Maxwell–Boltzmann distribution of linear and angular velocity with a random number generator. This caused the lattice to melt as the numerical integration routine took over the control and production of the individual molecular dynamical trajectories. The lattice took about 2000 time steps to melt into the liquid. When equilibrium was established the total energy became constant and negative, a sum of negative potential energy terms and positive kinetic energies of rotation and translation. In the liquid the two types of kinetic energy are numerically positive because they are measures of temperature in absolute (Kelvin) units. The potential energy in the liquid state is on the other hand negative because the sum of attractive parts of the pair potentials in the ensemble of 108 molecules is greater than the sum of positive, repulsive parts. The molecular liquid therefore stays together in a cohesive form such as that actually observed in a true liquid.

The next stage after achieving the liquid state and discarding the first 2,000 time steps or so needed for this was to implement further tests as follows.

P. Some Tests for the Liquid State

We have seen that at relatively long times or low frequencies, Eq. (1) should be valid for Brownian motion, the perpetual fluctuations in the position of a massive particle diffusing in an environment of much lighter molecules. One of the predictions[4] of Eq. (1) is that the mean-square displacement of the random walk in the position of the centre of mass of the Brownian particle depends linearly on time. One of the results of the 1964 simulation by Rahman was that this quantity was approximately linear far enough into the dynamical evolution from $t = 0$. Otherwise, shortly after $t = 0$, Eq. (1) is not at all applicable. This pattern was repeated for the simulation of dichloromethane. If the lattice has not melted properly the mean square displacement[181] is oscillatory, and more characteristic of the solid state.

Another test of melting was the computation of the orientational aver-

ages $\langle \mathbf{u}_1 \rangle$, $\langle \mathbf{u}_2 \rangle$, $\langle \mathbf{u}_3 \rangle$ over the three unit vectors in the axes of the principal molecular moment of inertia frame. In the isotropic liquid these all vanish, that is, the quantities actually simulated should fluctuate about a zero mean. If there are no special aligning effects caused by a positive Kirkwood factor, for example,[12] alignment caused by the interaction of molecular force fields, these averages should not fluctuate by more than about 0.1 either side of zero.

Finally, the center of mass positions of the molecules in the liquid state should show no solid like ordering, and averages over the center of mass positions in three dimensions should also fluctuate about a zero mean in the simulation.

Q. Thermodynamic Properties

Having made sure of melting the production runs were started, and ran for upwards of 10,000 time steps each. At each time step thermodynamic properties of the liquid were computed and at the end of 10,000 steps, averaged over the complete run for comparison with experimental data if available.

The basic quantities are temperature (T), pressure (P), and volume (V), whose interrelation defines the equation of state.[182] Even in the dilute gas the latter is in general an unknown quantity analytically, although there are numerous empirical representations. In view of this the direct measurement of deviations of real gases from the equation of state of the perfect gas

$$PV/T = \text{constant} \tag{113}$$

is represented in the virial expansion

$$\frac{pV}{T} = A + \frac{B}{V} + \frac{C}{V^2} + \cdots \tag{114}$$

due to Kammerlingh–Onnes. Here, A, B, and C are termed the first, second, and third virial coefficients and if known experimentally, are sensitive measures of the validity of the Lennard–Jones or any other representation of the pair potential and higher-order terms such as the three-body potential. The virial coefficient expansion is also applicable to other thermodynamic and dielectric properties of the dilute gas.[24] Ideally, computer simulation aims at reproducing known virial data from a given representation of the potential. However, there is at present a severe

shortage of experimental data on virial coefficients, which is a block to progress.

In the liquid the virial expansion is less useful, because many of its coefficients would be needed for the definition of the equation of the liquid state, and because there are severe fluctuations in the pressure from a molecular dynamics simulation at constant volume. This is a natural consequence of the fact that the mean intermolecular separation in the liquid is much less than in the dilute gas. The fluctuations in the Lennard–Jones potential energy function are inverse sixth and twelfth powers of this distance, and can therefore be very severe. The same is true of temperature, which is computed from the kinetic energies. The translational temperature is

$$T = \frac{1}{3Nk} \sum_{i=1}^{N} \mathbf{v}_i \cdot \mathbf{v}_i \tag{115}$$

The configurational part of the internal pressure, P_c, is computed from the virial coefficient ψ:

$$\langle P_c \rangle = \frac{N}{V} k \langle T \rangle - \frac{\langle \psi \rangle}{V} \tag{116}$$

where

$$\langle \psi \rangle = \left\langle \sum_{i<j} \sum r_{ij} \frac{\partial \phi_{ij}(r)}{\partial r_{ij}} \right\rangle + 2\pi \frac{N^2}{V} \int_{r_c}^{\infty} r^3 \phi'(r) g(r)\, dr \tag{117}$$

Here $\phi_{ij}(r)$ is the functional dependence of the Lennard–Jones pair potential on the interatomic distances (r) of the complete atom–atom potential between two molecules. $g(r)$ is the atom–atom pair distribution function, and is the numerical probability of finding an atom at a distance r from another of the same or different type given the initial position of the second atom. It is a measure of the liquid structure. N is the number of atoms in the sample, either of the same or different type as the case may be. The complete configurational contribution of the internal pressure is built up over all types of individual atom–atom contributions in Eqns. (116) and (117). V is the molar volume. The complete internal pressure of the sample is then given by eqn. (116) and the measurable thermodynamic pressure is

$$P = P_c - T\left(\frac{\partial P_c}{\partial T}\right)_{N/V} \tag{118}$$

This is the difference between two large and fluctuating numbers, and P as computed is therefore a small number with a large uncertainty. An expected pressure of 1 bar, for example, may be given numerically as something like

$$\langle P \rangle \simeq 1 \pm 300 \text{ bar} \tag{119}$$

Similarly, the configurational part of the internal energy is computed from

$$\langle U \rangle = \left\langle \sum_{i<j} \sum \phi_{ij} \right\rangle + U_c \tag{120}$$

where the sum is over all atom–atom pairs for which r_{ij} is less than a critical cut-off distance r_c. This necessitates the correction U_c based on a uniform distribution of molecules beyond:

$$U_c = 2\pi \frac{N^2}{V} \int_{r_c}^{\infty} r^2 \phi(r) g(r)\, dr \tag{121}$$

In the algorithm TETRA[1,2,4] for the simulation of dichloromethane, these principal thermodynamic quantities are computed at each time step, and an average produced at the end of the data production run in SI units. The algorithm also produces estimates of second-order thermodynamic properties such as specific heat, computed from fluctuations in first-order quantities.

R. Thermodynamic Results for Dichloromethane

The simulation algorithm should ideally produce the correct temperature and pressure for a given molar volume

$$V = \frac{M}{\rho} \tag{122}$$

which is the molecular weight divided by the liquid density. The pressure in particular is extremely sensitive to the individual atom–atom Lennard–Jones parameters σ and ϵ/k. The rotational and translational kinetic energies which produce the temperatures are also fluctuating quantities,

and in order to produce the correct temperature for a given input and molar volume (or liquid density), the sample must be thermostatted artificially, especially during the melting phase of the simulation. This is achieved with a routine known as temperature rescaling. The temperature is scaled back to the input value if the natural fluctuations exceed a given maximum, say $\pm 50\,K$. High-quality simulations avoid this procedure in production runs, and the temperature is allowed to fluctuate naturally. In the melting stage, however, very large artificial temperature fluctuations may be unavoidable because of molecules becoming artificially entangled or crushed together during the melt process, as the ensemble finds its optimum equilibrium configuration.

In the simulation of the test dichloromethane molecule[2,4] the optimized Lennard–Jones potential illustrated already produced the following pressure and temperatures for an input molar volume corresponding to 293 K and 1 bar.

1. The mean temperature was 294.5 ± 11 K (50.2% translational and 49.8% rotational), compared with the experimental value expected at 293 K.
2. The mean pressure was 273 ± 300 bar.
3. The computed specific heat at constant volume was 46 J mole^{-1} K^{-1}; compared with the experimental value[2] of 90 J mole^{-1} K^{-1}.

The thermodynamic properties computed for this relatively small sample of 108 dichloromethane molecules are in fair agreement with the true experimental values, but by no means perfect. Given the approximations and uncertainties used throughout the exercise, the agrcement is acceptable, and typical of contemporary simulations.

S. Dynamical and Spectral Properties[1,2,4]

Having produced numerical results for basic thermodynamic properties of liquid dichloromethane in reasonable agreement with the limited amount of experimental data available, the next step is to use the same trajectories to attempt to match the experimental spectral properties of the liquid. These are characterised briefly as in Section II by various types of radiation absorption, dispersion, and scattering.

T. Microwave and Far Infrared Absorption and Dispersion

These cover a range of about three frequency decades equivalent to the sub-picosecond to nanosecond time range. In comparing the simulations with available experimental data[1,2,4] in pure dichloromethane liquid, there

are complications which must be borne in mind. These include the following:

1. The time correlation function from the experimental microwave data is the multiparticle ccf of orientation[183]

$$C_u(t) = \left\langle \sum_i \sum_j \mathbf{u}_i(0) \cdot \mathbf{u}_j(t) \right\rangle \tag{123}$$

which is related through an equation such as (19) of Section I to the Fourier transform of the dielectric loss, and its second time derivative

$$C_{\dot{u}}(t) = \left\langle \sum_i \sum_j \dot{\mathbf{u}}_i(\mathbf{0}) \cdot \dot{\mathbf{u}}_j(t) \right\rangle \tag{124}$$

essentially[1] the Fourier transform of the far infrared power absorption coefficient. Limited availability of computer time and storage meant that only the acf's equivalent to Eqs. (123) and (124) were within range of the computation. These are $\langle \mathbf{u}(0) \cdot \mathbf{u}(t) \rangle$ and $\langle \dot{\mathbf{u}}(0) \cdot \dot{\mathbf{u}}(t) \rangle$. Their Fourier transforms will only approximate the observed spectra[1,2] because of the missing intermolecular cross correlations. However, these may be removed by dilution in a nondipolar solvent such as carbon tetrachloride,[1,2,4] which is observed experimentally to shift the complete far infrared power absorption (second spectral moment) to lower frequencies. Proceeding on the assumption that the dilute solution contains less dynamical cross correlation between dichloromethane molecules than in a pure liquid of the latter, a comparison[1,2] with the data from the simulation can be made. The result is sketched in Fig. 11. Here the maxima of the observed and simulated spectra have been adjusted to be the same for ease of comparison of the frequency dependence. The validity of this procedure is discussed in point 2 below. The figure shows reasonably good agreement. In view of the approximations inherent in our computer simulation of the pure liquid, the result is an advance over the theory of Section I. For example, the far infrared absorption peak, clearly defined in the interferometric data obtained experimentally in terms of the far infrared power absorption coefficient, is also clearly present in the computer simulation from a simple Fourier transform of the dipole moment (μ) rotational velocity acf $\langle \dot{\mu}(t) \cdot \dot{\mu}(0) \rangle$. The simulated power absorption coefficient also regains transparency at high frequencies. The simulation is therefore more realistic than the original theory of rotational diffusion, which produces plateau absorption, and also its counterpart corrected for inertial effects,

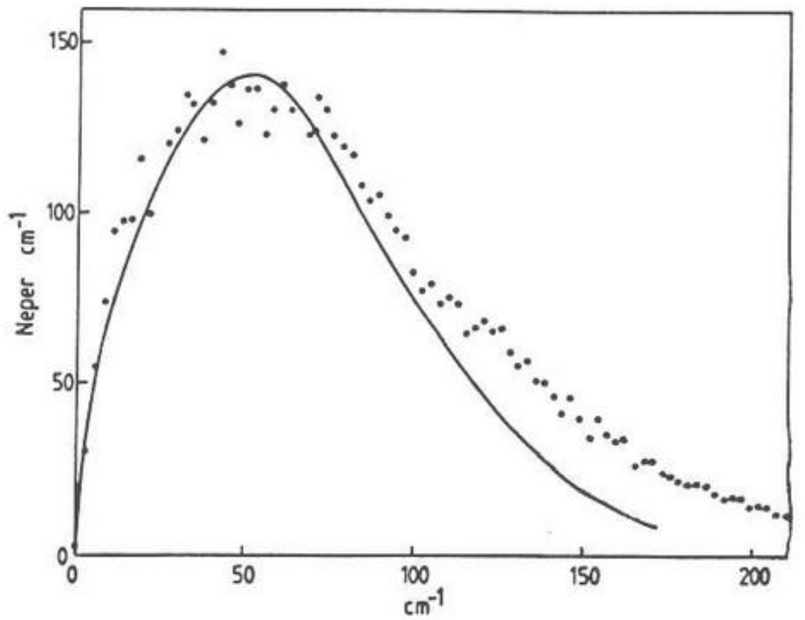

Figure 11. Comparison of simulated and far infrared power absorption of liquid dichloromethane. ● Simulation; — experimental data.

which merely produces a far too gradual fall-off from this plateau. The simulated peak position agrees well with that experimentally observed in a dilute solution of dichloromethane in carbon tetrachloride, chosen to try to remove inter-molecular cross correlations[1,12] between dichloromethane molecules in the neat liquid. Despite the agreement in Fig. 11 it may be objected that the comparison is between a computer simulation of the pure liquid dichloromethane, with cross correlations unaccounted for due to lack of computer availability, and an experimentally derived dilute solution of dichloromethane in carbon tetrachloride. These are valid criticisms which can be met only with increased computer time. The latter is needed both to compute the full intermolecular ccf's (123) and (124) and to simulate directly a solution of dichloromethane in carbon tetrachloride. For a 10% solution with about 108 dichloromethane molecules this would require about 900 carbon tetrachloride molecules. Such large-scale computations would still be faced, of course, with a contemporary lack of ab initio potentials, our limitation to classical equations of motion, and artificial removal of many-body effects in our current approach to computer simulation. In the meantime, of particular interest in Fig. 11 are the high- and low-frequency ends of the spectrum. At high frequencies the observed power absorption coefficient of the dilute solution regains transparency more quickly than the simulated counterpart. This is because the simulation relies on a finite Taylor-series expansion of the type sketched briefly

in this chapter. At some point in these Taylor expansions the next higher time derivative is left out as the series is truncated. This implies (Section II) that spectral moments will cease to be definable at some stage. These effects are visible in the simulated second moment (the power absorption coefficient) through the relatively slow decay to transparency of the simulated data in comparison with the experimental observation. The fourth spectral moment is defined in TETRA, because the code defines the time derivative of the mean-square torque, but the sixth moment from the simulation will not regain spectral transparency at high frequencies. This emphasizes that the simulation is an imperfect numerical approximation to the classical equations of motion assumed to govern molecular dynamics. In view of the uncertainty axioms[184–186] of quantum mechanics, operable at subpicosecond time scales, this assumption is itself of limited validity. At low frequencies in Fig. 11 the traditional microwave[12,24] and far infrared ranges overlap. The traditional measure (Section I) of microwave absorption is the dielectric loss and dispersion, and the Debye relaxation time. The dielectric loss is simply another way of expressing the power absorption coefficient through Eq. (16) of Section I. It is also affected by the same cross correlations as those in the far infrared, and these appear implicitly in Eq. (123). A complete computer simulation of the dielectric loss must include these and would proceed over about 50,000 time steps out into the nanosecond range (GHz frequency range). This combination of requirements, together with the need for a 5.0-fs time step to maintain the stability of the total energy in the simulation[91,145] needs an investment of computer time. The original simulation of dichloromethane[2,4] was severely limited by lack of computer availability which restricted the computation of Eq. (123) to the acf, and then only out to about 2.0 ps (400 time steps). At 2.0 ps into its time evolution the acf had fallen[2] to about one-third of its initial value, normalized to 1.0 at $t = 0$, as is the contemporary practice. The time dependence of the acf in this intermediate range (from about 0.2 to the available limit of 2.0 ps) closely approximated an exponential. At longer times (50.0 ps or more) we would expect to see a long time tail (Eq. 111). In the face of these limitations it is reasonable to proceed approximately with the definition of a correlation time from the computer simulation at the instant when the correlation function has decayed to $1/e$ of its value at $t = 0$. This is approximately comparable with the Debye relaxation time, bearing in mind that both times involve autocorrelations only. This procedure gave 1.2 ps from the computer simulation compared with an observed[1] dielectric relaxation time of 1.45 ps. The latter is defined simply as the inverse of the peak frequency of the dielectric loss. The neglect of intermolecular cross correlations in the simulation yields a relaxation time which is too short and a

far infrared power absorption peak frequency ($55.0\,cm^{-1}$) which is too low in comparison with the observed peak frequency[1,2] in pure liquid dichloromethane of $80.0\ cm^{-1}$. In many respects, however, the computer simulation is an improvement over the theory of rotational diffusion. For example, it is carried out in three dimensions, using the proper asymmetric top molecular structure, a fairly realistic model pair potential, and involves both translational and rotational diffusion simultaneously. The trajectories are able to provide a range of thermodynamic and spectral data self-consistently.

2. A further complication not accounted for explicitly in the computer simulation is that of the internal field correction. This occurs[12,24] in all spectral observations of the molecular liquid state for dielectric materials. The correction tries to determine the effective or internal field felt by a diffusing molecule as opposed to the applied field intensity. In dielectric relaxation[12,24] the applied measuring field is often an alternating electric field at a given frequency, or a klystron generator. In the far infrared it is broad-band radiation from a high-pressure mercury lamp, for example. In all cases the diffusing molecule is shielded from the full intensity of the radiation by the fields of other molecules in the sample. The problem of determining the effective internal field is dependent on the molecular dynamics that are being investigated by spectral means. In computer simulation, there is no probe field and time correlation functions are built up directly, without an intervening Fourier transformation. Any comparison of simulation and spectrum must involve, however, a correction of the spectral data for the internal field. There are several literature approaches[1] designed to adjust for the frequency dependence of the internal field correction (the dynamical internal field). The most generally valid approaches are based on the Mori approximation to the Liouville equation developed in the 1970s. The procedures are not entirely unequivocal, however, because use is made of the traditional approach of Section I within the framework of the correction. The argument is circular, the theory of diffusion is used to correct spectra intended to give information on the same theory of diffusion. The circle can be broken, however, as exemplified in Refs. 187 and 188. The micro–macro theorems[1] are easier to apply to practical problems, but at the expense of empiricism introduced by approximants of the Mori continued fraction. An example of one of these theorems[189] is outlined in Ref. 1. As a rule of thumb the various internal field corrections do not have a large effect on the frequency dependence of the far infrared power absorption,[190] but can alter the Debye relaxation time by pushing the peak frequency of the theoretical dielectric loss downwards in frequency by as much as about half a decade.

The correction has a large effect, however, on the intensity of the far infrared and dielectric spectra.[12] This correction is significant whether or not frequency dependent. The typical effect of the Polo–Wilson correction,[1,191] for example, is to reduce the intensity of the spectrum by about 25% over the complete frequency range. This means that the field effective on a diffusing molecule is weaker on the average by about a quarter than that originally applied at the boundary of the sample by the spectroscopist. It is convenient to normalize the far infrared power absorption obtained experimentally to the peak of the same curve obtained in a computer simulation, on the assumption that the internal field correction does not significantly distort the frequency dependence of the spectrum. This allows a comparison such as that of Fig. 11.

3. Another uncertainty in comparing spectrum and simulation is introduced by collision-induced effects coming from the mutual distortion of molecular electron clouds in ensembles. These effects can be dramatic in the far infrared under particular combinations of circumstance. This was shown clearly by Baise[72] in compressed gaseous and liquid nitrous oxide, a weakly dipolar molecule whose electron distribution is easily prone to distortion by other nitrous oxide molecules. The theory of collision induced absorption involves considerations of higher multipole moments of the distribution of electronic charge.[192] These quantities are obtained by a Taylor expansion akin in symmetry to the spherical harmonics.[24] The point charge is a scalar, the dipole moment a vector, the quadrupole moment is a tensor with nine components; the octopole moment has 27 components and the hexadecapole moment 81. The quantum theory of multipole-induced dipole absorption in the far infrared[1] predicts quantum lines spaced by $\Delta J = 2$ for quadrupole-induced dipole absorption, $\Delta J = 3$ for octopole-induced dipole absorption, and so on, where J is the rotational quantum number. In practice the "lines" are almost always broadened into bands which are superimposed on the high-frequency side of the far infrared absorption due to the permanent dipole itself. Baise[72] observed a large effect of multipole induced dipole absorption in nitrous oxide and further effects[65–67] have been isolated due to dipole-, quadrupole-, and octopole-induced dipole absorption in the halogenated hydrocarbons such as fluorotrichloromethane with dipole moments in the intermediate range. The present author isolated the hexadecapole moment of oxygen using its far infrared absorption.[193] Fortunately for the study of diffusion processes characterized solely by the permanent dipole moment of the molecule, the induced effects go through a maximum in the moderately compressed gas, but thereafter decrease due to symmetry,[72] because the arrangement of nearest neighbors on the average leads to a cancellation of multipole-induced absorption. In a molecular crystal, the cancellation is sometimes complete and collision-induced spectra vanish. In preparation for the European Molecular Liquids Group pilot project on dichloromethane, account was taken of the fact that the area beneath the power absorption coefficient in the far infrared of this strongly dipolar species is an experimentally observed linear function of number density (N) in dilute solutions.[1] Multipole effects evidently assume a secondary role, because they are nonlinear in N. Dichloromethane is therefore a good choice for the comparison of data from simulation with those from the far infrared. Nevertheless, collision-induced absorption or scattering is always present, theoretically, and some computer simulations[194] have addressed the problem directly.

U. Infrared Absorption

This technique produces correlation times which are usually assumed to relate directly to the acf of the transition dipole moment of the absorption. For dichloromethane, early work[194] produced a correlation time for the axis of the permanent dipole of only 0.5 ps, much shorter than the 1.2 ps from the simulation by Ferrario and Evans[2,4] and shorter than the dielectric relaxation time of 1.45 ps. This is one illustration of the fact that cross correlation between vibration and rotation must be understood properly in infrared absorption bands broadened by liquid diffusion. Contemporary uncertainty is further illustrated by the fact that an independent investigation[195] of the same infrared information produced a correlation time of about 1.2 ps, in close agreement with the simulation.

V. Relaxation of Nuclear Magnetic Resonance

By collecting data in liquid dichloromethane from a number of different types of nuclear magnetic resonances it is possible to arrive at correlation times[114] for different axes of the molecule fixed frame (x, y, z). For any orientation vector $\mathbf{u}$ the correlation function is a second rank Legendre polynomial, which is most simply expressed as

$$P_2(t) = \tfrac{1}{2}\langle 3(\mathbf{u}(t)\cdot\mathbf{u}(0))^2 - 1\rangle \tag{125}$$

For the axis defined by the H–H vector in the dichloromethane molecule the correlation time is 0.53 ps from relaxation of resonance of the proton nucleus.[114] From deuterium quadrupole relaxation[114] the correlation time for the C–D axis is 0.80 ps. The correlation time for the diffusion of the C–H axis is 0.70 ps,[114] from C–H dipole nuclear magnetic resonance relaxation. From Cl nuclear magnetic resonance quadrupole relaxation the relaxation time for the diffusion of the C–Cl axis is 1.20 ps. These

experimental results were collected by Brier and Perry[114] and show an anisotropy of the molecular diffusion process which was successfully reproduced by Ferrario and Evans[2,4] by computer simulation. The latter produced 0.5 ps for the correlation time of the acf (Eq. 125) of the dipole unit vector, and 0.90 ps for the correlation time of the perpendicular axis of the principal moment of inertia frame. The equivalent of the H–H correlation time from the computer simulation was found to be 0.51 ps. Although there is broad agreement about the anisotropy of the diffusion process, there is internal discrepancy among experimentally derived correlation times.[114] The computer simulation is more effective than the traditional approach to this problem, which relies on three empirical and unknown friction coefficients within an inadequate theoretical framework.

W. Depolarized Rayleigh Scattering

The orientational correlation function from depolarised Rayleigh scattering from liquid dichloromethane complements the data available from a combination of far infrared and microwave spectroscopy. However, the orientational time correlation function from Rayleigh scattering is the second-order Legendre polynomial of Eq. (125). In general, data from depolarised Rayleigh scattering contain contributions from collision-induced effects[195] of the type discussed already in this chapter for the far infrared absorption spectra of dipolar liquids. The process of data reduction to provide a correlation time characteristic of the diffusion of an axis of the dichloromethane molecule must therefore take into account the presence of cross correlations and collision-induced effects.[195] There is a further practical problem in depolarized light scattering as compared with the far infrared in that the intensity of the depolarised scattered light falls very rapidly to the baseline,[117–120] being essentially equivalent to a zero spectral moment. In shape, the frequency dependence of Rayleigh scattered radiation is approximately equivalent[117] to $\alpha(\omega)/\omega^2$, that is, the far infrared power absorption divided by ω^2. This is essentially speaking dielectric loss divided by ω. We have seen in (Section I) that dielectric loss is relatively insensitive to high-frequency molecular dynamics and it follows that raw Rayleigh scattering data are even less so. In actual experimental data the information of most interest to molecular dynamics is contained in the far wing of the Rayleigh scattering profile at frequencies from about 5–300 wavenumbers from the frequency of the exciting line of the laser radiation with which the sample is probed for its light scattering characteristics.[117–120]. Collision-induced effects (dependent on the interaction of two or more molecules) are also more pronounced[195] in Rayleigh scattering than in far infrared absorption because the former depends

TABLE I
Comparison of Observed and Computer Correlation Times for Liquid Dichloromethane

Technique	Axis	Correlation Time (ps)
NMRH	H–H	0.53 ± 0.06
NMRD	C–D	0.80 ± 0.10
NMR C–H	C–H	0.70 ± 0.07
NMR Cl	C–Cl	1.20 ± 1.10
Computer simulation, P_2	$\mathbf{u}_1$	0.5
	$\mathbf{u}_2$	0.9
	$\mathbf{u}_3$	0.5
Neutron scattering	H (cm)	0.56
Dielectric relaxation	$\mathbf{u}_1$	1.45
Infrared	$\mathbf{u}_1$	0.5
	$\mathbf{u}_1$	1.1
Computer simulation, P_1	$\mathbf{u}_1$	1.2
	$\mathbf{u}_1$	3.8
	$\mathbf{u}_3$	1.2
Rayleigh scattering	$\mathbf{u}_1$	1.85

directly on the polarisability tensor of Eq. (71) and the latter on the dipole moment vector.

Despite these complications van Konynenberg and Steele[195] have obtained a correlation time from depolarized Rayleigh scattering at one temperature and pressure. This is the second Legendre correlation time of the dipole moment axis, and was found to be 1.85 ps. This is in marked disagreement, however, with the computer simulation of Ferrario and Evans,[2,4] which produced 0.5 ps for the equivalent correlation time, approximating much more closely to the N.M.R. relaxation time.[114]

X. Incoherent, Inelastic Neutron Scattering

The neutron-scattering data obtained by Brier and Perry[114] were analysed by them in terms of several models of the liquid state, but were insufficiently varied or accurate to produce a reliable picture of the molecular diffusion process. This is a contemporary problem with neutron scattering and the interpretation of such data would benefit from routine computer simulation.

Y. Survey of Correlation Times

A survey of correlation times from the various data sources available is provided in Table I for liquid dichloromethane. The autocorrelation times from the computer simulation and the NMR relaxation produce a picture of anisotropic diffusion, which is corroborated by the results from infrared spectroscopy. A combination of the multiparticle correlation times from

dielectric relaxation (1.45 ps) and depolarized Rayleigh scattering (1.85 ps) shows that the theory of rotational diffusion cannot explain the data satisfactorily, because the theory requires the latter to be three times shorter than the former. The equivalent autocorrelation times from the computer simulation are 1.2 ps and 0.5 ps respectively, the opposite trend to that from the dielectric and Rayleigh scattering data.

The anisotropy of the diffusion process is shown by the fact that the correlation time for diffusion of the dipole axis from the simulation is 1.2 ps, while that for the principle moment of inertia axis parallel to Cl–Cl is 3.8 ps. The same trend is observed in the correlation times from infrared analysis, but the absolute values in the latter case are shorter (0.5 and 1.1 ps). From NMR relaxation the same anisotropy is observed from the proton relaxation time, (H–H axis) of 0.53 ps and the chlorine quadrupole relaxation time (1.30 ps, C–Cl axis). The anisotropy in the equivalent second-order relaxation times from the computer simulation is expressed as 0.5 and 1.1 ps, respectively. There is therefore overall agreement but not in detail.

In particular the correlation time from depolarized Rayleigh scattering is anomalous, and the neutron scattering results equivocal. Table 1 shows however that computer simulation is far more effective than the theory of Section I in explaining all the available data coherently. The same simulation trajectories can produce a variety of new information (Sections V, VII, and VIII) unavailable to conventional spectral investigation.

Z. A Survey of Molecular Liquids

The methodology sketched in this section of comparing a range of spectral and thermodynamic data for the same liquid with computer simulation has been applied in several cases. The interested reader is referred to the specialist literature[4] and to source papers for more details:

1. The symmetric tops chloroform,[196] methyl iodide,[197] and acetonitrile[198] in the liquid state.
2. The symmetric tops bromoform[199] and *t*-butyl chloride[200] in the liquid and rotator phases.
3. The asymmetric tops acetone[201] and ethyl chloride[202] in the liquid and supercooled states.
4. The H-bonded asymmetric tops water[203–206] and methanol.[207]
5. The spherical tops carbon tetrachloride,[56,57] germanium tetrabromide,[208] carbon tetrabromide,[208] phosphorus,[208] and sulphur hexafluoride.[208]
6. The chiral asymmetric tops bromochlorofluoromethane,[209] 1,2-dimethylcyclopropane,[210,211] fluorochloroacetonitrile,[212–214] and others.[215–220]
7. Plate-like and rod-like molecules.[221]

In all cases the computer simulation povided a broad range of data from the same set of trajectories, and also investigated new ccf's of many different types. This has been achieved in the last decade and is an advance over the state of understanding summarized in Section I.

IV. SIMULATION – NEW RESULTS

In the last decade computer simulation has produced many new and fundamental results on molecular diffusion processes. These have made obsolete many of the analytical ideas of Section I. We have seen in Section III that computer simulation can be used to describe a range of experimental information given a representation of the pair potential incorporated in the classical equations of motion. Having tested the technique against experimental data in this way, it is reasonable to apply it to probe the limits of applicability of the basic analytical ideas. Some of the simulation results are fundamentally important, and the analytical approach of Section I is still struggling to come to terms with the new numerical advances. Similarly, the computer simulations have been able to predict the outline results of key spectral data, giving a more profound and specific picture of the molecular liquid state and its dynamical properties. Before embarking on a description of these results, it is necessary to define some basic statistical concepts and techniques of utility.

A. Linear Response Theory and the Fluctuation–Dissipation Theorem

One of the clearest approaches to understanding the linear response approximation in the theory of diffusion is to consider thc diffusion equation used originally in the Debye theory of 1913. This equation was derived from a Smoluchowski equation governing the evolution in time of a conditional probability density function $f_2(x_2, t_2 \mid x_1, t_1)$ of the random variable x. The product $f_2\, dx_2$ is the probability that $x(t_2)$ has a value in the range $(x_2, x_2 + dx_2)$ given that $x(t_1)$ had the value x_1 at t_1. A random variable[1] is a dynamical quantity that may take any of the values of a specified set with a specified relative frequency or probability. In molecular dynamics it can be a vector quantity such as centre-of-mass linear velocity or, as in the Debye equation, an angular variable. It is defined through a set of permissible values to each of which is attached a probability. The Smoluchowski equation is derived by considering the probability density function (pdf) $f_3(x_3, t_3 \mid x_1, t_1)\, dx_3$ which is the probability that the random

variable $x(t_3)$ has the range of values $(x_3, x_3 + dx_3)$ given that $x(t_2)$ has the value x_2 at time t_2 and that $x(t_1)$ has the value x_1 at time t_1.

To find the pdf $f_3(x_3, t_3 | x_1, t_1)$ we have to multiply f_2 and f_3 and average over all possible values taken by x_2. This averaging process can be considered as integration, from the basic laws of integral calculus. This leads directly to the Chapman–Kolmogorov equation[222]

$$f_3(x_3, t_3 | x_1, t_1)\, dx_3 = \int_{-\infty}^{\infty} f_2(x_2, t_2 | x_1, t_1)\, f_3(x_3, t_3 | x_2, t_2; x_1, t_1)\, dx_2 dx_3 \tag{126}$$

The Smoluchowski equation is derived from this equation by making the additional assumption that the conditional pdfs

$$f_3(x_3, t_3 | x_2, t_2; x_1, t_1) = f_2(x_3, t_3 | x_2, t_2) \tag{127}$$

The Smoluchowski equation is therefore

$$f_2(x_3, t_3 | x_1, t_1) = \int_{-\infty}^{\infty} f_2(x_2, t_2 | x_1, t_1) f_2(x_3, t_3 | x_2, t_2)\, dx_2 \tag{128}$$

In the context of molecular diffusion, the Markov hypothesis is equivalent to approximating the memory function of Eq. (6) of Section I with a time-independent friction coefficient, which appears in the rotational Langevin equation (Eq. 27). The physical consequence of this "loss of memory" is that Markov theory loses its ability to describe the far infrared power absorption coefficient.

B. Taylor Expansion of the Smoluchowski Equation

An analytical solution of the Smoluchowski equation can be approximated by expanding the pdf's which appear on both sides of Eq. (128) in Taylor series. This is achieved with the variable $z = x_3 - x_2$, fixing x_2. Writing $t_2 = t$ and $t_3 = t + \delta t$, we have

$$f_2(x_3, t_3) = f(x_3, t + \delta t) = \int_{-\infty}^{\infty} f(x_2, t)\, f(x_3, t + \delta t | x_2, t) dx_2 \tag{129}$$

The variable x_3 determines z because x_2 is fixed, that is, given a finite value with probability 1. This implies

$$f(x_3, t + \delta t | x_2, t) = q(z, \delta t | x_2, t) \tag{130}$$

Assuming that q is independent of the value x_2 from which the transition is made and independent of the time t_2,

$$f(x_3, t + \delta t | x_2, t) = q(z, \delta t) \tag{131}$$

Equation (129) now becomes

$$f(x, t + \delta t) = \int_{-\infty}^{\infty} q(z, \delta t) f(x - z, t)\, dz \tag{132}$$

It is now assumed that $f(x, t + \delta t)$ and $f(x - z, t)$ have well-defined Taylor expansions:

$$f(x - z, t) = f(x, t) - z \frac{\partial f(x, t)}{\partial x} + \frac{z^2}{2!} \frac{\partial^2 f(x, t)}{\partial x^2} + \cdots \tag{133}$$

and

$$f(x, t + \delta t) = f(x, t) + \delta t \frac{\partial f(x, t)}{\delta t} + \frac{(\delta t)^2}{2!} \frac{\partial^2 f(x, t)}{\partial t^2} + \cdots \tag{134}$$

Finally, the Smoluchowski equation as used by Debye is obtained by assuming that the time interval δt is very small. This leads to

$$\frac{\partial f(x, t)}{\partial t} = \frac{1}{2!} \frac{\langle z^2(\delta t) \rangle}{\delta t} \frac{\partial^2 f(x, t)}{\partial x^2} \tag{135}$$

Making use of the averages

$$D = \lim_{\delta t \to 0} \frac{1}{2} \frac{\langle z^2(\delta t) \rangle}{\delta t} \tag{136}$$

and

$$\langle z^2(\delta t) \rangle = \int_{-\infty}^{\infty} z^2 q(z, \delta t)\, dz \tag{137}$$

finally leads to

$$\frac{\partial f}{\partial t} = D\frac{\partial^2 f}{\partial x^2} \tag{138}$$

which is the form of the Smoluchowski equation used as the starting point of Debye's theory of 1913 and of Einstein's theory of 1905. The diffusion coefficient (Section I) is

$$D = \frac{kT}{6\pi\eta a} = \frac{kT}{m\beta} \tag{139}$$

and Eq. (138) is an approximation to the integral equation (Eq. 129) for the pdf:

$$f(x, t \,|\, x_1, t_1) = f(x, t) \tag{140}$$

Equation (138) is derived from the very simple framework of the Chapman–Kolmogorov equation (Eq. 126).

Note that Eq. (138) refers to the pdf of position only. A more complete analysis refers to both velocity and position simultaneously, and is known as the Fokker–Planck equation.[1–4] It governs the conditional probability of finding the molecule both with a given position and velocity at time t_1, given both its position and velocity at t.

C. The Concept of Linear Response

If the diffusing molecule is subjected to an external or internal potential energy barrier, the approximation (Eq. 138) must be modified. For the sake of simplicity we consider linear diffusion in one axis. The analytical representation of the molecular diffusion under the influence of a potential $V(x)$ is

$$\frac{\partial f}{\partial t} = \frac{kT}{m\beta}\frac{\partial^2 f}{\partial x^2} + \frac{1}{\beta}\frac{\partial}{\partial x}\left(\frac{\partial V(x)}{\partial x} f\right) \tag{141}$$

D. Rotational Diffusion

Equation (141) was adopted by Debye for rotational diffusion in two dimensions of a molecular dipole moment subjected to an external time-varying electric field **E**. In this case $f(\theta, t)\, d\theta$ is the number of dipoles whose axes lie in an element $d\theta$ on the circumference of a circle. The

pdf is a function of the angle θ between the dipole and the field. The Smoluchowski equation for this process is[1,2,4]

$$\frac{\partial f(\theta, t)}{\partial t} = \frac{\partial}{\partial \theta}\left(\frac{kT}{\zeta}\frac{\partial f(\theta, t)}{\partial \theta} + \frac{1}{\zeta}\frac{\partial V(\theta, t)}{\partial \theta} f(\theta, t)\right) \tag{142}$$

where ζ is the rotational friction coefficient. This equation corresponds to the Langevin equation with the inertial term missing. The statistical process described by the Smoluchowski equation (Eq. 142) involves instantaneous jumps in the angular motion of the dipole axis. The pdf involves position only, and not angular velocity, so that the equation is said to be written in configuration space.

These historical approximations illustrate the meaning of linear response if we write the potential between dipole and field as

$$V = -\mu E \cos\theta = -\boldsymbol{\mu}\cdot\mathbf{E} \tag{143}$$

at Eq. (142) becomes

$$\frac{\partial f(\theta, t)}{\partial t} = \frac{\partial}{\partial \theta}\left(\frac{kT}{\zeta}\frac{\partial f(\theta, t)}{\partial \theta} + \frac{\mu E}{\zeta}\sin\theta f(\theta, t)\right) \tag{144}$$

This is an equation valid for rotation about fixed axes only, but if the dipoles are also free to rotate in space then it is modified for use in spherical polar coordinates, f being now the pdf governing the number of dipoles whose axes point in an element of solid angle Ω. The three dimensional equation is

$$\frac{\partial f(\Theta, t)}{\partial t} = \frac{1}{\sin\Theta}\frac{\partial}{\partial \Theta}\left[\sin\Theta\left(\frac{kT}{\zeta}\frac{\partial f(\Theta, t)}{\partial \Theta} + \frac{\mu E}{\zeta}\sin\Theta f(\Theta, t)\right)\right] \tag{145}$$

where $f(\Theta, t)\sin(\Theta)\, d\Theta$ is the probability that at time t the dipole has an orientation between Θ and $\Theta + d\Theta$ relative to $\mathbf{E}(t)$; and $M(\Theta, t) = \mu E \sin\Theta$ is on the torque on the dipole due to the applied field. Equation (145) is a special case of the Smoluchowski equation:

$$2\tau_D \frac{\partial f}{\partial t} = \mathrm{div}\left[\mathrm{grad}\, f + \frac{f}{kT}\mathrm{grad}\, V\right] \tag{146}$$

E. Solution for Arbitrary Field Strength

Analytical solutions for arbitrary field strength are available[1–4] only with simple forms, such as the rectangular pulse

$$\mathbf{E}(t) = \mathbf{E}_0(U(t) - U(t - t_1)) = \mathbf{E}_0 e(t) \tag{147}$$

where $U(t)$ is the unit step function. The solution of Eq. (145) is assumed to take the general form[223]

$$f(\Theta, t) = \sum_{n=0}^{\infty} a_n(t) P_n(\cos\Theta) \tag{148}$$

where P_n are the Legendre polynomials and a_n are to be determined. The Legendre polynomials have the orthogonality[224]

$$\int_{-1}^{1} P_n(x) P_m(x)\, dx = \frac{2}{2n+1}\delta_{m,n} \tag{149}$$

The ensemble averages defining the system are

$$\langle P_n(\cos\Theta)\rangle = \frac{\int_{-1}^{1} f(\Theta, t) P_n(\cos\Theta)\, d(\cos\Theta)}{\int_{-1}^{1} f(\Theta, t)\, d(\cos\Theta)} = \frac{a_n(t)}{a_0(2n+1)} \tag{150}$$

and these can be computed from Eq. (145) to any order in $\cos\Theta$ following Ref. 1, pp. 151 ff. The first two rise transients are then (for $t < t_1$)

$$\langle P_1\rangle_R = \frac{1}{3}\left[\gamma(1 - e^{-t/\tau_D}) - \frac{1}{5}\gamma^3\left(\frac{1}{3} - \frac{te^{-t/\tau_D}}{2\tau_D} - e^{-2t/\tau_D} - \frac{1}{4}e^{-t/\tau_D}\right) + \cdots\right] \tag{151}$$

$$\langle P_2\rangle_R = \frac{1}{5}\gamma^2\left[\left(\frac{1}{3} - \frac{1}{2}e^{-t/\tau_D} + \frac{1}{6}e^{-3t/\tau_D}\right)\right] + \cdots \tag{152}$$

and the fall transients after switching off the fields instantaneously at $t = t_1$ are

$$\langle P_1\rangle_F = \frac{1}{3}\gamma(e^{-(t-t_1)/\tau_D} - e^{-t/\tau_D}) - \frac{1}{15}\gamma^3\left(\frac{1}{3}e^{-(t-t_1)/\tau_D} - \frac{t_1}{2\tau_D}e^{-t/\tau_D} - \frac{1}{4}e^{-t/\tau_D} - \frac{1}{12}e^{-(t-t_1)/\tau_D}\right) + O(\gamma^5) \tag{153}$$

$$\langle P_2\rangle_F = \frac{1}{5}\gamma^2\left[\frac{1}{3}e^{-3(t-t_1)/\tau_D} + \frac{1}{6}e^{-3t/\tau_D} - \frac{1}{2}e^{-t/\tau_D}e^{-2(t-t_1)/\tau_D} + O(\gamma^4)\right] \tag{154}$$

It can be seen from these equations that the rise and fall transients are mirror images (Section I) only when terms linear in $\gamma = \mu E_0/(kT)$ are retained. This is the approximation first given by Debye and is a consequence of the linear response approximation.

Another is that in the linear response limit the fall transient is an exponential, and has the same time dependence as the orientational acf from the equivalent Langevin equation (Eq. 8) of Section I. Finally, the rise and fall transients cease to be functions of the field strength only in the same linear response regime, $\gamma^3 \ll \gamma$.

These linear response approximations are assumed implicitly in the relation of spectral band shapes to time-correlation functions. In the theory of dielectric relaxation, for example,[12] the field strength does not enter into consideration, because implicit in the theory is the fluctuation-dissipation theorem

$$\frac{\langle P_1\rangle_F}{\langle P_1\rangle_0} = \frac{\langle\cos\Theta(t)\cos\Theta(0)\rangle}{\langle\cos\Theta(0)\cos\Theta(0)\rangle} \tag{155}$$

that is, the fall transient's time dependence is the same as that of the equilibrium acf in the linear response approximation. The acf is defined at field-free reversible thermodynamic equilibrium. In dielectric relaxation the field is in general frequency-dependent, from subradio frequencies to the far infrared.

F. Computer Simulation of Rise and Fall Transients in an Arbitrarily Strong External Field — Violation of the Linear Response Theory

The theory given above, due originally to Coffey and Paranjape,[223] gave the first indication of what would happen if linear response were inapplicable. Roughly contemporaneously, several experimental indications of the limits of linear response were obtained,[24,225–227] but a full theoretical

description remains intractable. This is due essentially to the fact that the Smoluchowski equation (Eq. 145) is for configurational space only, and there is no proper definition of the role of angular velocity. The appropriate equation for the space of configuration and velocity is the Kramers equation.[1–4] The latter corresponds to a Langevin equation with inertial and potential terms on the left-hand side, akin to Eq. (32) of Section I, or the itinerant oscillator equations (Eqs. 36 and 37). In general, the Kramers equation must be solved by numerical differential differencing, and this is possible only in idealized cases.[1–4]

A much more direct and practical approach to the exploration of nonlinear response theory, and of nonlinear problems in general, is computer simulation.

G. Computer Simulation in an Applied External Field

This technique was devised[2,3,160,228] in the early 1980s and prompted fundamental changes in our appreciation of diffusion processes. The basic idea is an adjustment to the forces loop (Chapter (3)) of a standard constant volume algorithm such as TETRA. The extra torque $-\boldsymbol{\mu} \times \mathbf{E}$ is coded into the algorithm at the point where the net intermolecular torque is computed from the forces. The extra torque is switched on at the arbitrary initial $t = 0$ and the main simulation algorithm starts to respond. Extra information is provided numerically which can be compared with any available analytical theory, however rudimentary the latter may be, through the careful investigation of (1) rise transients, (2) fall transients, and (3) field-induced acf's and ccf's.

H. Rise Transients

Equilibrium orientation averages such as those represented by Eqs. (151)–(154) are produced in the computer simulation by monitoring the effect of the extra torque on a simple average (over the number of molecules in the sample) of the unit vector $\mathbf{u}_1$ in the axis of the molecular dipole moment $\boldsymbol{\mu}$ or any other definable axis in the molecule. In the absence of the aligning field averages such as these vanish, because the sample is isotropic. Optical properties such as the refractive index are the same on average in each axis X, Y, or Z of the laboratory frame. However, when the electric field is applied, and the extra torque between field and dipole takes effect, each molecule becomes partially aligned on average in the field direction: the sample is polarized and becomes birefringent. The complex permittivity (ϵ) and the complex refractive index (n) are linked by

$$\epsilon(\omega) = [n(\omega)]^2 \tag{156}$$

so that any directional phenomenon such as polarization (a field-dependent change in the complex permittivity) is accompanied by an equivalent effect in the complex refractive index. The microscopic quantity equivalent to these observable effects on permittivity and refractive index after the field is switched on is the rise transient, the average $\langle \mathbf{u}_1(t) \rangle_R$ as a function of time t.

I. The Langevin Function

The rise transient eventually reaches a value at which it fluctuates about a mean value greater than zero. This final level is dependent on the torque generated between field and dipole and therefore on the extra energy imparted by the applied electric field. An illustration for several field strengths is given in Fig. 12. An analytical description of the dependence of the level reached by the transient on thc applied electric field was first derived by Langevin and is known as the Langevin function. It is expressed in terms of the ratio $b = \mu E/(kT)$ (Section I). For the first-order rise transient $\langle \mathbf{u}_1(t) \rangle_R$ the Langevin function is

$$L_1(b) = \frac{e^b + e^{-b}}{e^b - e^{-b}} - \frac{1}{b} \tag{157}$$

The second-order rise transient described analytically in Eq. (152) has its equivalent Langevin function also:

$$L_2(b) = 1 - \frac{2L_1(b)}{b} \tag{158}$$

These analytically derived Langevin functions are plotted against the saturation values of rise transients from computer simulation in Figs. 13 and 14. The computer simulation reproduces the Langevin functions[2,3] for the test molecule dichloromethane treated with strong electric fields, sufficient to saturate the functions. This would be difficult experimentally[24] owing to heating effects, sparking, and difficulty in generating the huge electric field strengths required. The numerical simulation, having been checked out in Section III, produces information on Langevin functions of all orders. This takes us into unknown territory, that of nonlinear dielectric spectroscopy, unexplorable with contemporarily available electric field strengths, and inaccessible to anything but the most rudimentary of analytical theories.

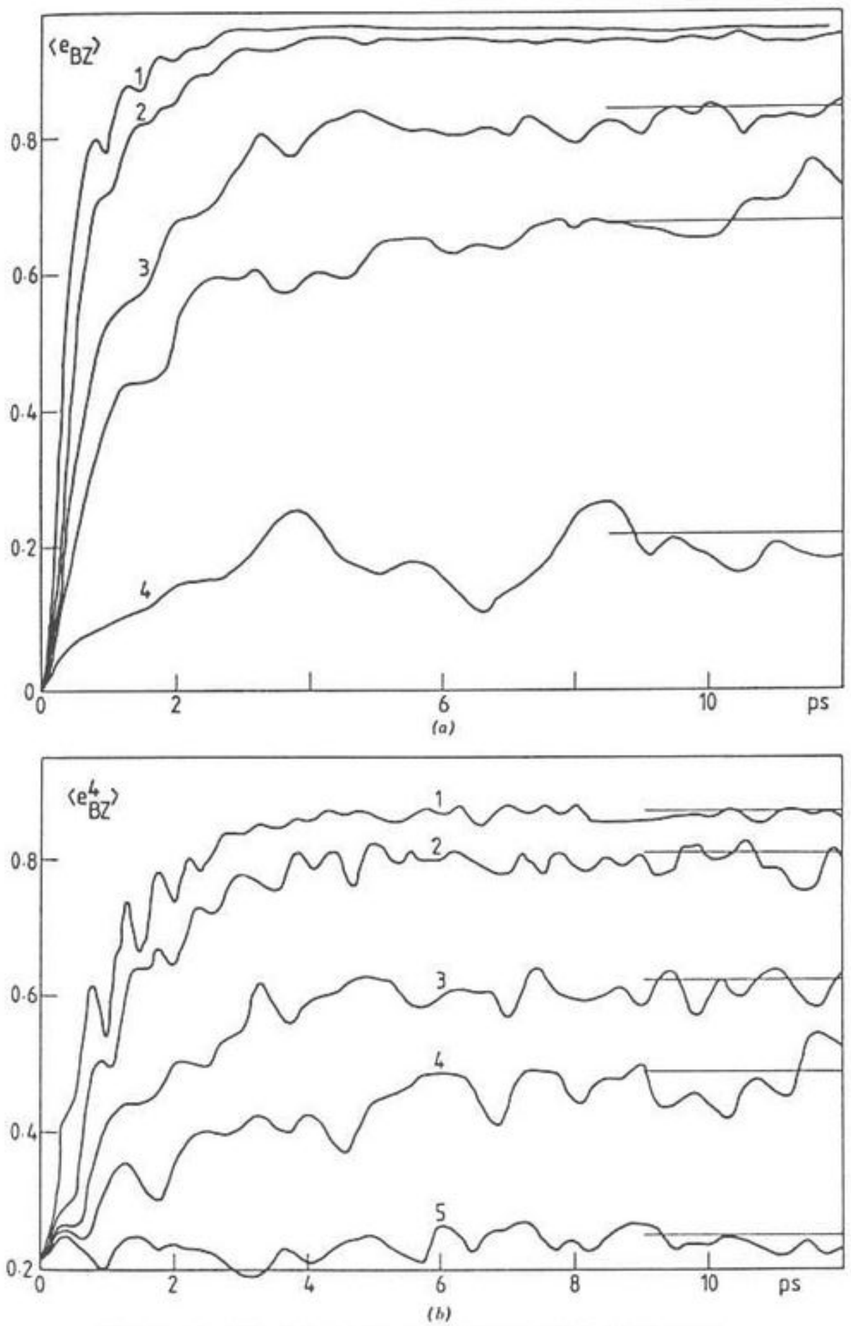

Figure 12. Rise transients as a function of field strength.

J. Time Dependence of the Rise Transient

The Langevin functions of order $n = 1$ to m are available analytically because they are simple thermodynamic averages.[9] The time dependence

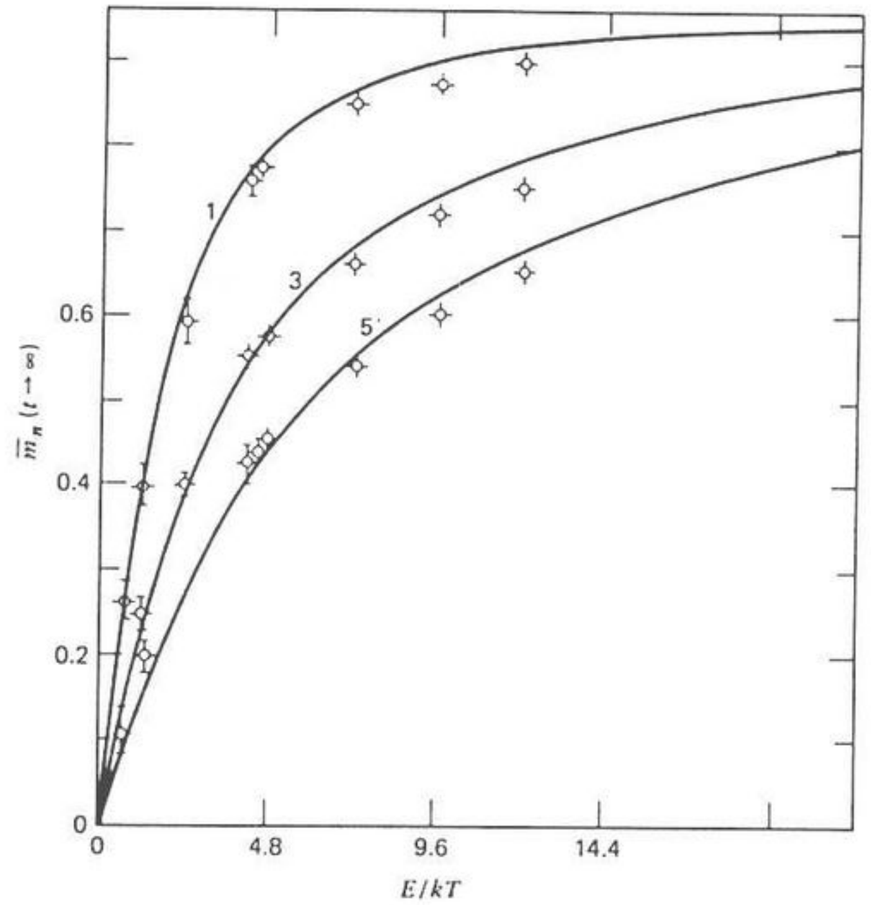

Figure 13. Langevin functions at first, third, and fifth order (full lines) plotted against plateau levels from computer simulation (symbols).

of the transient is much more difficult to obtain. The results of Coffey and Paranjape [223] were among the first to be obtained outside the confines of linear response, but are nevertheless derived in configurational space only, from a simple Smoluchowski equation. They carry with them all the inherent flaws of the customary theory of diffusion. Even in this case Eqs. (151)–(154) are series approximations, sufficient only to show that the rise and fall transients are no longer mirror images. As soon as linear response is left behind, the transients become field-dependent. What little is known analytically shows only that the transients are in general dependent on the approximation employed for the intermolecular potential energy, again a departure from the results in the linear response approximation. The analytical representation of the intermolecular potential in diffusion theory is woefully inadequate. For example, the rise transient may be obtained from a Langevin equation[229]

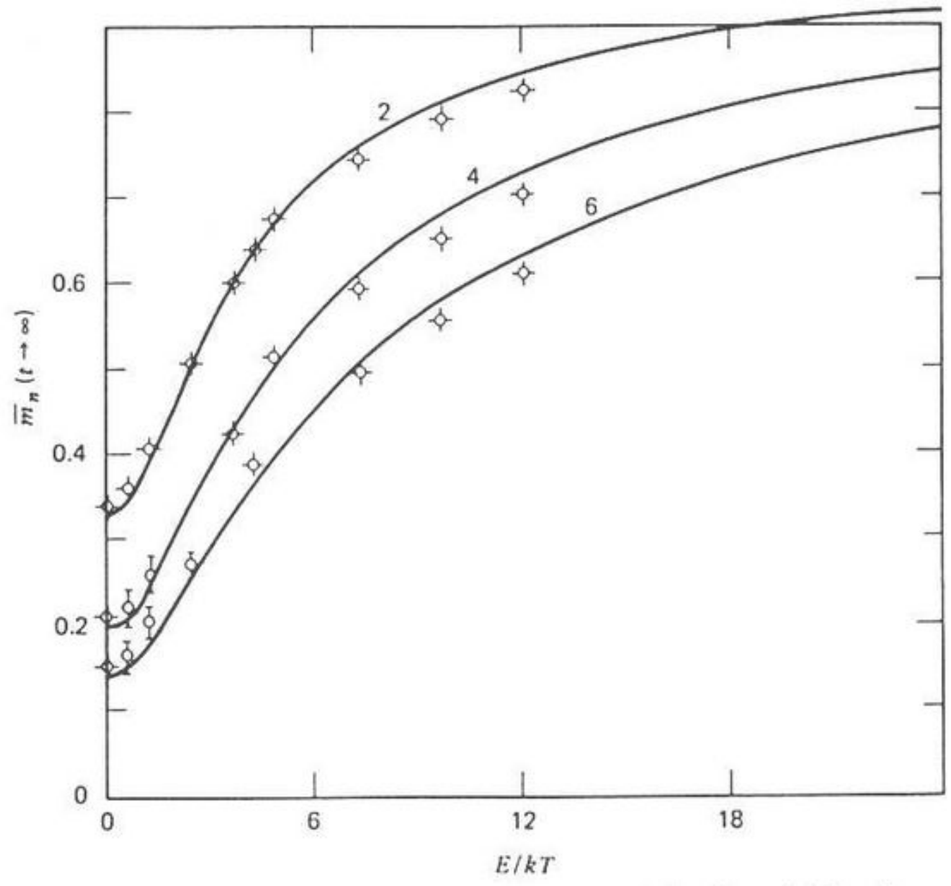

Figure 14. As for Fig. 13, Langevin functions at second, fourth, and sixth order.

$$I\ddot{\theta}(t) + \zeta\dot{\theta}(t) + E_0 \sin\theta(t) = \lambda(t) \tag{159}$$

The inertial term is present in this equation and makes a startling difference to the time dependence of both the rise and fall transients, as illustrated in Figs. 15 and 16. The Langevin equation (Eq. 159) must be transfomed to the equivalent Kramers equation, however, and is insoluble as it stands. The results from the Kramers equation are obtained numerically, by standard differential differencing, and cannot be obtained analytically. The presence of the inertial term and extra torque term on the left-hand side of Eq. (159) have profound effects on the rise transient, making it markedly oscillatory, and accelerate the decay of the fall transient. These indications have been matched by computer simulation[230] in liquid water, using a more realistic representation of the pair potential. Figures 17 and 18 illustrate the oscillations in the rise transient from the simulation, which considered 1372 water molecules. The simulated oscillations are dependent on the electric field strength and the pattern of oscillations is

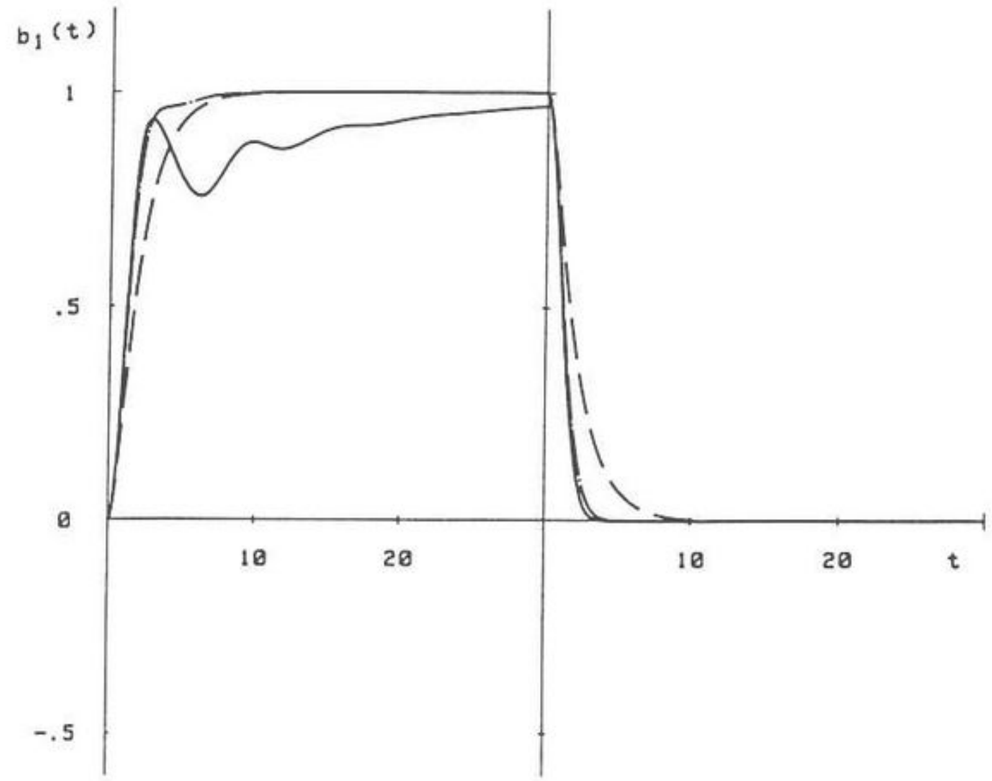

Figure 15. First-order rise and fall transients obtained from the work of Coffey et al., ref. (229).

dependent on the model used of the intermolecular pair potential. This means that experimental information on the potential can be obtained in principle from observations of oscillatory rise transients. This is a critically important simulation result, verifying the analytical indications, and leading to a new method of investigating the pair potential. The field strengths necessary to achieve this are available not in electric fields but in the electric field components of laser fields, applied in trains of very short-lived but extremely powerful pulses. The pair potential in this simulation was modelled with a 5×5 site–site representation devised by the present author.[203–206] It is probable that a different rcpresentation of the water pair potential (or triplet and higher-order potentials)[151] would produce a different pattern of oscillations, and thus provide a practical method of differentiating between different model and ab initio potentials.

The restriction to two-dimensional diffusion (Eq. 159) are removed in the simulation. Both the two- and three-dimensional approaches give the same overall indications.

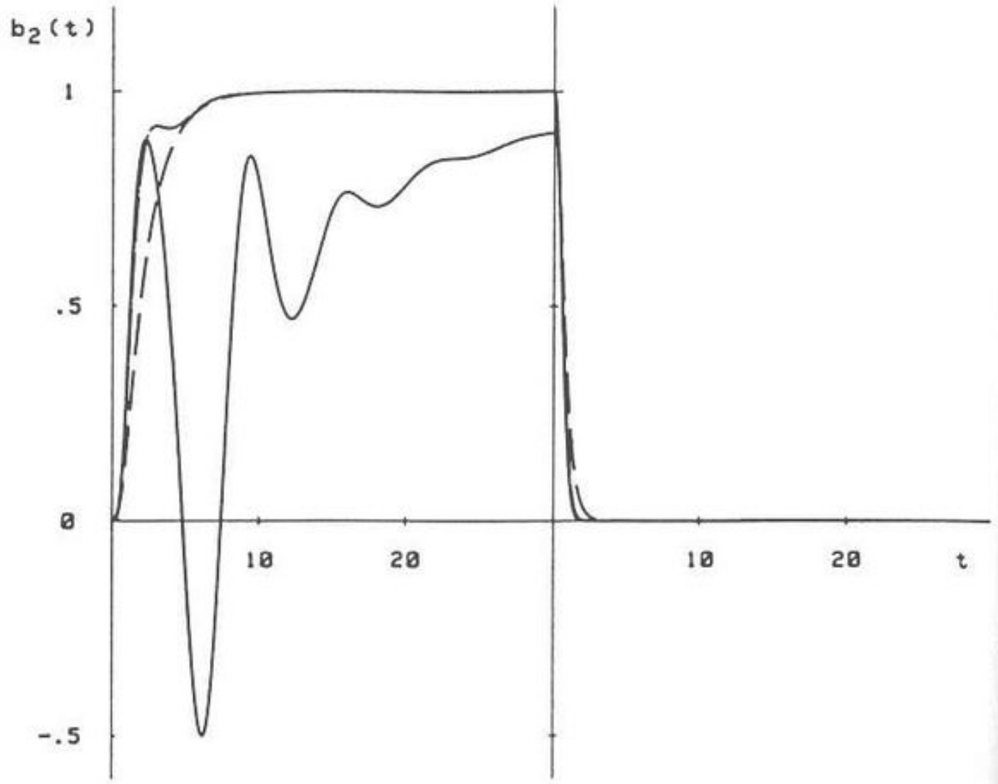

Figure 16. As for Fig. 15, second-order rise transients.

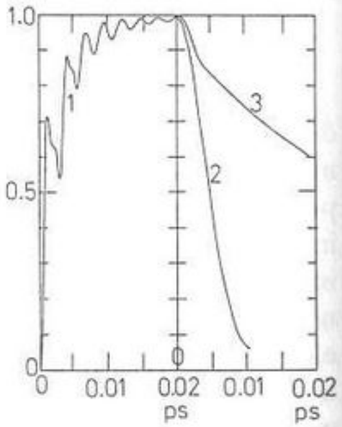

Figure 17. Rise and fall transients from computer simulation of 1372 water molecules, illustrating rise-transient oscillation and fall transient acceleration for a given electric field strength, ref. (230).

K. The Fall Transient

Agreement in principle has also been achieved between computer simulation and analytical theory concerning the time dependence of the fall transient. In linear response theory this is simply the mirror image of the rise transient, both being exponentials which are identical with the normalised equilibrium acf

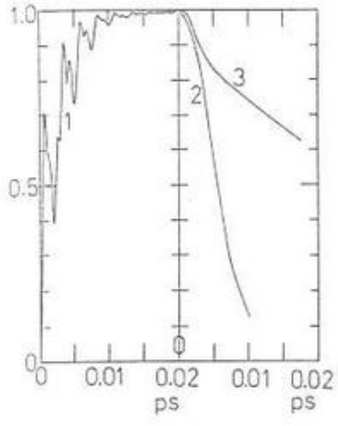

Figure 18. As for Fig. 17, varying the field strength. The oscillation and acceleration effects are dependent on field strength.

$$\frac{\langle \mathbf{u}_1(t)\rangle}{\langle \mathbf{u}_1(0)\rangle_{t=0}} = \frac{\langle \mathbf{u}_1(t)\cdot\mathbf{u}_1(0)\rangle}{\langle \mathbf{u}_1(0)\cdot\mathbf{u}_1(0)\rangle_{E=0}} \tag{160}$$

Equations (153) and (154), from the relatively simple model of the Debye diffusion equation, show that the fall transient has a complicated time dependence, involving the field strength. The fall transient can decay more quickly to zero than the field-free equilibrium acf. This was first discovered[228] in a computer simulation of liquid dichloromethane in 1982. The simulation was followed by an analytical confirmation.[229] Similar analytical work[231,232] was reported later which again showed the same result. The new effect was identified as fall transient-field acceleration, and later appeared in several corroborative simulations[3,230–232] The most important likely consequence is the use of the effect in the experimental investigation of the intermolecular potential, using intense laser pulse trains. In so doing the individual time dependencies of both the rise and fall transients must be describable consistently by the same representation of the potential energy between molecules. This can only be achieved by computer simulation back-up, because the analytical appreciation is still severely limited. However, analytical theory has managed to show that the effect is produced only when the dependence of the model potential on the angular variable is nonlinear, as for example in Eq. (159). The harmonic approximation $\sin\theta \simeq \theta$ does not produce a fall transient acceleration. This is contrary to the findings of several computer simulations, and the harmonic approximation must be discarded. This conclusion is consistent with the fact that the far infrared power absorption coefficient of a liquid such as dichloromethane needs for its rudimentary description an effectively nonlinear potential representation. Fall-transient acceleration is a fundamental property of the molecular liquid state and any analytical description which fails to describe it must be modified. The

same is true of far infrared power absorption. Ideally, both sources of information should be treated by the same computer simulation, as in our work on the test liquid dichloromethane.

Fall-transient acceleration results specifically from the nonlinear nature of the effective potential energy and is also dependent on the applied electric field strength.

L. Correlation Functions in the Field on Steady State

We havc seen that the Debye–Smoluchowski equation is derived by applying the Markov approximation to the Chapman–Kolmogorov equation. The Markov approximation therefore underlies the Langevin equation, for example, Eq. (8) of Section I. Reinstating the inertial term modifies the nature of the diffusion process, so that the Smoluchowski equation in configuration space must be replaced by the Fokker–Planck equation in the space of both configuration and velocity. The extension of the phase space in this way leaves unaffected, however, thc basic Markov assumption uscd in attempting to solve Eq. (126), and also leaves unaffected the truncation of the Taylor expansions Eqs. (133) and (134). Much of the analytical work in exploring the ramifications of these approximations has occurred in the last decade,[3] and is constantly spurred on by the findings of computer simulation.

One major shortcoming of the Markov approximation is the failure of the resultant Langevin equation, with or without inertial terms, to describe the observed far infrared power absorption coefficient. The Liouville equation does not, furthermore, reduce straightforwardly to the Langevin equation, and this is also due to the Markov approximation. This was made particularly clear by Mori, using projection operators. These produced the Liouville equation in the form Eq. (6) of Section I, a form which resembles the Langevin equation, but reduces to it only if the Mori resonance operator vanishes and the memory function is a delta function, the friction coefficient of Langevin. The latter has no time dependence because it is a consequence of the Markovian exclusion of the statistical influence of historical events upon the time evolution of the molecular dynamical ensemble.

The experimental indications such as far infrared spectra suggest that the liquid state is non-Markovian in nature. Past events affect the statistical nature of future events, and the Markov approximation (Eq. 127) is too severe.

One of the clearest signs of this non-Markovian nature is the field-decoupling effect anticipated by Grigolini[233] and confirmed[3] by the present author with computer simulation.

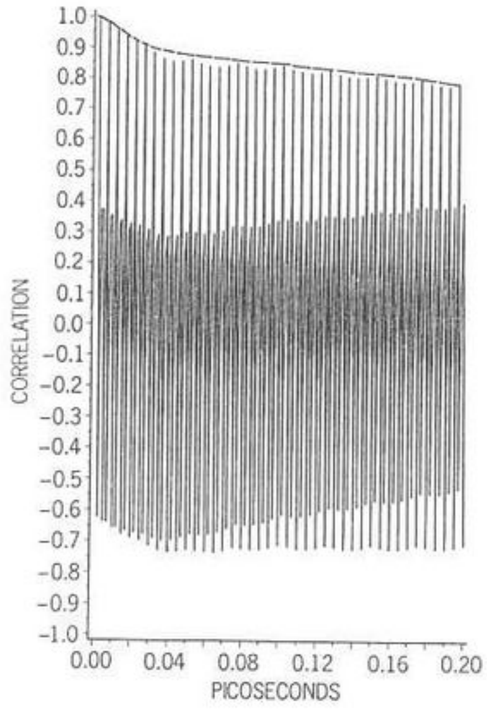

Figure 19. Illustration of the decoupling effect, the field-induced envelope marked by the dashed line decays more slowly than the equivalent field-off acf due to the liquid's inherently non-Markovian statistical nature. (Water, right C.P. laser, first order torque. Rotational velocity ACF'S, F = 400 THZ, field = 6000.)

M. The Decoupling Effect

When a molecular liquid sample is treated with an intense uniaxial electric field, some of the acf's in the ensemble become oscillatory. The frequency of the oscillations is governed by the torque $-\boldsymbol{\mu} \times \mathbf{E}$. They are often most pronounced in the angular velocity acf, and the decoupling effect relates to the envelope of the time decay of the field-induced oscillations. The rate of decay of this envelope, marked by the dashed line in Fig. 19, is considerably slower than the loss of correlation in the field-free acf, and the greater the field strength, the slower the decay of the envelope.

To explain this consistently with fall-transient acceleration and far infrared absorption it is necessary to abandon the Markov approximation completely. The friction coefficient in an equation such as Eq. (159) must be replaccd by a memory function, which has time dependence. The analytical theory must be upgraded once more in response to advances made by computer simulation to the point where it is minimally capable of describing the information available. This new level of description is represented by

$$I\ddot{\theta}(t) + \int_0^t \phi(t-\tau)\dot{\theta}(\tau) + E_0 \sin\theta(t) = \lambda(t) \tag{161}$$

with the memory function ϕ. This equation can describe the decoupling effect qualitatively, and also the fall-transient acceleration, oscillations in the rise transient, and the rudiments of far infrared absorption.

This upgrading of the analytical theory will no doubt continue in the future as more is discovered by computer simulation. The theory of diffusion of Section I is clearly, therefore, not a complete theory which can stand on its own and make predictions in terms of the fundamental physical constants. It is not a quantum theory or a Newton theory of motion in bodies. Numerical simulation is clearly able to provide something more, to anticipate the existence of new physical phenomena. Diffusion theory not only finds itself incapable of prediction, but is also unable to describe available data, especially when judiciously combined. Some examples are given next of the findings of the simulation method.

N. New Type of Birefringence

A material is birefringent if its refractive index in one axis (say X) is different from those in Y and Z. Birefringence can occur naturally, as in a molecular crystal or aligned nematogen[1] or can be induced in a normally isotropic liquid by an external field of force,[9] mechanical, electrical, magnetic, electromagnetic, and others.

O. The Kerr Effect[9]

In the Kerr effect the inducing field is an electric or electromagnetic field, whose effect can now be understood through the imposed torque $-\boldsymbol{\mu} \times \mathbf{E}$ on each molecule. It can be investigated experimentally with great accuracy.[234] The development of the birefringence as a function of time (the rise transient), and its loss after switching off the field (the fall transient), can be measured. Diffusion theory[223] provides a limited appreciation of these results, which are available usually at relatively low frequencies. Both the traditional experimental[234] and theoretical[9] methods associated with the time-dependent Kerr effect failed completely to detect rise-transient oscillations and fall-transient acceleration. The theoretical approaches failed to realize the importance of inertial and nonlinear terms, took insufficient account of memory effects, and relied too much on low frequency data. There are purely experimental restrictions[24] due to weak aligning fields and limitation to low frequencies. However, if these can be remedied, and the use of computer simulation intensified, Kerr effect relaxation may become a less superficial means of investigation than at present.

P. The Cotton–Mouton Effect

The induction of birefringence in this case takes effect with an external magnetic field, and this is a strong effect in liquid crytals. Much less is reported about the effect of an aligning magnetic field in isotropic, molecular, liquids. The alignment takes effect through the torque generated by the magnetic dipole and magnetic field. The strength of the effect depends on the magnetic dipole, whether this is diamagnetic or paramagnetic. The new superconducting materials[235] offer scope for the generation of very intense magnetic fields with which to develop this technique for use with isotropic molecular liquids.

Q. Birefringence Induced with Electromagnetic and Neutron Radiation

Electromagnetic and neutron radiation induce birefringence, the former is sometimes known as the optical Kerr effect, but neutron-beam induced birefringence is not yet developed experimentally

R. Flow-Induced Bifringence

In a flowing molecular liquid, the birefringence parallel and perpendicular to the axis of flow is measurably different, and this problem can now be tackled by large scale computer simulation.[4,91,145] Similarly, rotational or vortex flow in a molecular liquid leads to birefringence.

S. Birefringence Effects Discovered by Computer Simulation

The development of new computer architectures, at IBM and elsewhere, has allowed the exploration of bigger samples in molecular dynamics computer simulation and improvements in the statistical quality of the runs. Partly as a result of this new found power and computer time, new birefringence phenomena have been discovered numerically. These are described as follows with reference to liquid water, simulated with the author's 5×5 site–site potential.

T. Electric-Field-Induced Translational Anisotropy

Computer simulation takes us outside the limitations of linear response and rotational diffusion, and opens the door to new exploration[235]. The use of a simple torque of the type $-\boldsymbol{\mu} \times \mathbf{E}$ has resulted in the numerical discovery of new effects, which the traditional approach of Section I cannot describe. One of the most revealing of these is the induction of birefringence in the linear centre of mass velocity acf in response to an applied electric field. At field strengths outside the range of linear response and conventional dielectric relaxation, this acf develops a different time dependence perpendicular and parallel to the applied electric field. This

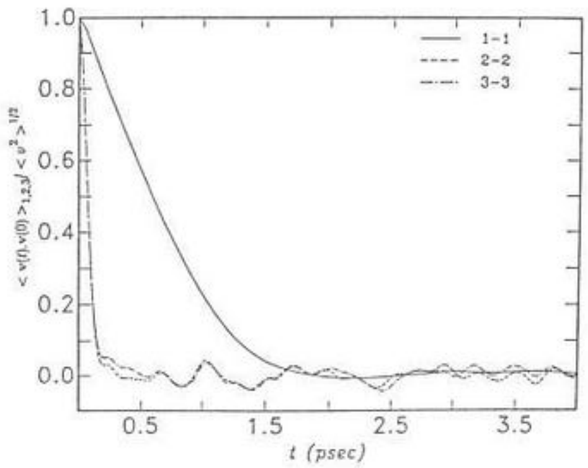

Figure 20. Computer simulation of electric field induced anisotropy in the acf of the molecular centre of mass in liquid water.

was known neither experimentally nor theoretically prior to the computer simulation[235] which produced the result illustrated in Fig. 20. An applied torque of the type $-\boldsymbol{\mu} \times \mathbf{E}$ results in different rates of translational diffusion parallel and perpendicular to the field, although there is no net flow in the sample. This result is a new measurable phenomenon of the liquid state which marks the boundary beyond which rotational diffusion theory cannot go. A purely rotational Mori theory (Eq. 161) cannot be used to describe this development. Translational variables such as the molecular center of mass linear velocity simply do not appear in our "upgraded" equation (Eq. 161). An imposed *torque* has resulted in anisotropy of *linear* velocity. Nothing in the purely rotational theory of this chapter, dependent on the Debye–Smoluchowski approach, and its more realistic rotational relatives, could have predicted the result obtained numerically and shown in Fig. 20.

This reveals a major flaw in the analytical description of molecular diffusion, one which can be traced directly to the original assumptions made independently by Einstein and Debye. Both assumed that the two fundamental modes of diffusion in a rigid dipolar molecule, rotation and translation, can be dealt with independently. There were sound reasons for this at the turn of the century (Section I), but Fig. 20 shows that rotational and translational effects are interrelated. A purely rotational or purely translational description of the molecular liquid state is insufficient. There are many new things to explore once this is realized, and some of these are described later in this chapter. Computer simulation is in advance of both analytical theory and experimental investigation in being the first

technique to produce an unexpected result such as electric field induced anisotropy in the translational diffusion process.

U. Birefringence Induced by a Circularly Polarized Laser

Experimental exploration of the effects of intense electric fields must rely contemporaneously[236] on laser pulses, in which the electric and magnetic field components are described classically by Maxwell's field equations. One of the easiest ways of appreciating how the laser field can interact with a liquid of dipolar molecules is by considering again the simple torque $-\boldsymbol{\mu} \times \mathbf{E}$. This time, the electric field comes from the Maxwell equations of the complete electromagnetic laser field. The electric component of the laser field sets up the torque through interaction with the molecular dipole moment (the antenna which picks up the laser radiation). This introduces new possibilities, for example, the use of a circularly polarized laser field of the type

$$E_X = 0 \tag{162}$$

$$E_Y = E_0 \cos \omega t \tag{163}$$

$$E_Z = E_0 \sin \omega t \tag{164}$$

The components of the torque set up by the laser are then

$$\boldsymbol{\mu} \times \mathbf{E} = \begin{vmatrix} \mathbf{i} & \mathbf{j} & \mathbf{k} \\ \mu_X & \mu_Y & \mu_Z \\ 0 & E_0 \cos \omega t & E_0 \sin \omega t \end{vmatrix} \tag{165}$$

Incorporating these into the forces loop of TETRA produces new information about the way in which an intense laser field can interact with a molecular ensemble to produce new and measurable ccf's in the laboratory frame (X, Y, Z), and from these new information on the molecular dynamics. This information is beyond the boundaries of the traditional approach because a torque of the type in Eq. (165) makes the equations of rotational diffusion completely intractable. Once we depart from linear response theory, there is no closed solution[223] for the Debye–Smoluchowski equation, as described earlier in this chapter. The computer simulation method, on the other hand, deals with the laser field through a simple extra torque coded in to the algorithm. More complicated forms of torque can also be utilized straightforwardly.

A recent simulation of the effect of a strong circularly polarized laser[236]

has revealed a range of new results using an intense pulse of radiation. The simulation was carried out on liquid water in three dimensions using 1372 molecules. Good statistics were obtained with 6000 time steps of 0.5 fs each. All 6000 time steps were implemented to build up time correlation functions by running time averaging. These were computed in the steady state obtained after the sample had come to equilibrium in the presence of the laser. In this steady state, new cross-correlation functions appeared directly in the laboratory frame (X, Y, Z) exemplified by

$$\mathbf{C}_1^{ij}(t) = \frac{\langle \boldsymbol{\mu}_i(t)\boldsymbol{\mu}_j(0)\rangle}{\langle \mu_i^2\rangle^{1/2}\langle \mu_j^2\rangle^{1/2}} \tag{166}$$

The diagonal elements of this tensor make up the usual acf of the water molecule's dipole moment, that is, the orientational acf related through a Fourier transform such as Eq. (19) to the dielectric loss. The computer simulation showed that this acf becomes anisotropic in the presence of the intense laser field, that is, its components in (X, Y, Z) develop a different time dependence (Fig. 21). This shows the laser inducing a first order birefringence in the molecular liquid. The refractive index in the axis of the applied laser is different from those in the two mutually perpendicular axes. This follows from the relation between dielectric permittivity and refractive index, the former being related by Fourier transformation to the orientational acf.

This birefringence develops without any consideration of the molecular polarizability, which results in the extra torque

$$-(\mathbf{E}\cdot\boldsymbol{\alpha}\cdot\mathbf{E})\times\mathbf{E} \tag{167}$$

on each molecule, where a is the molecular polarizability tensor. Considerations of the second order torque (Eq. 167) leads to a second order birefringence phenomenon. The effect in Fig. 21 is to first order in the electric field component of the laser, and was unknown prior to the computer simulation. This illustrates the predictive ability of computer simulation in areas where the customary approach has become ineffective due to analytical intractability or where experimental investigation has not been initiated.

The simulation is also capable of providing detailed supplementary information from the same set of molecular trajectories built up over 1372 molecules and 6000 time steps. This information is exemplified in Fig. 22, which shows that the off-diagonal elements of the tensor (Eq. 166) are stimulated to exist directly in frame (X, Y, Z) by the circularly polarized laser. Any future analytical description must take this finding into account,

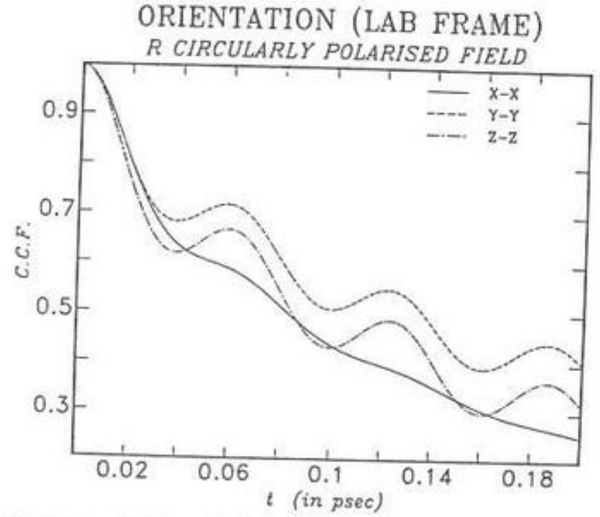

Figure 21. Anisotropy in the dipole orientational acf of liquid water induced by a circularly polarized laser.

and experimentally, these new ccf's are capable of direct observation. Similar results appear in the computer simulation of the tensor of the rotational velocity

$$\mathbf{C}_2^{ij}(\mathbf{t})_{XYZ} = \frac{\langle \dot{\boldsymbol{\mu}}_i(t)\dot{\boldsymbol{\mu}}_j(0)\rangle}{\langle \dot{\mu}_i^2\rangle^{1/2}\langle \dot{\mu}_j^2\rangle^{1/2}} \tag{168}$$

illustrated in Figs. 23 and 24. This means that the far infrared power absorption coefficient of the liquid water sample perpendicular and paral-

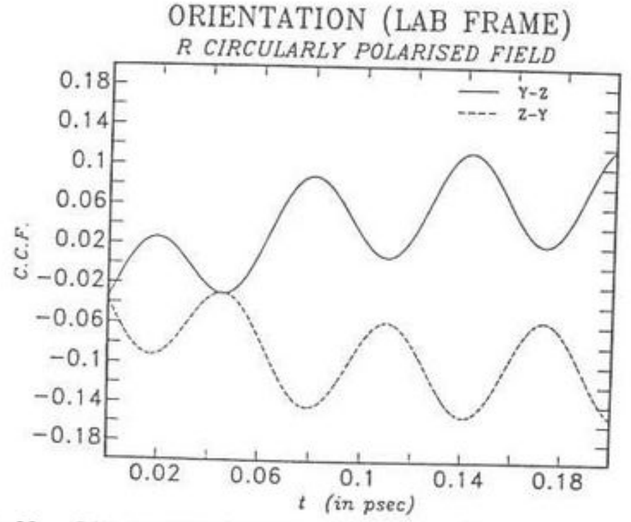

Figure 22. Off-diagonal elements of the tensor illustrated in Fig. 21.

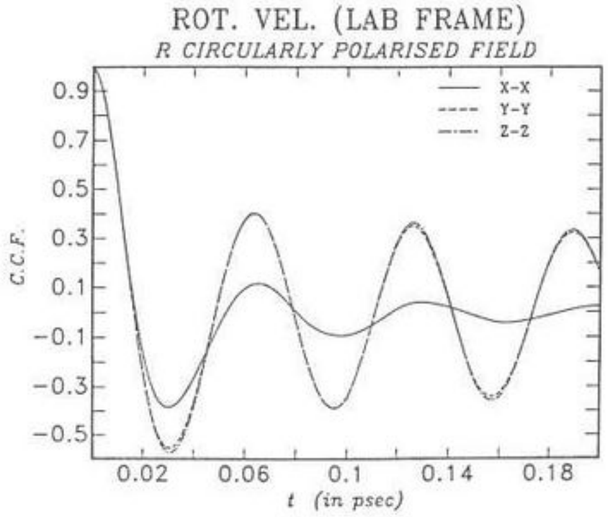

Figure 23. As for Fig. 21, rotational velocity acf.

lel to the applied laser field will become different in frequency dependence, together with the refractive index at these frequencies. There is birefringence both at high (far infrared) and low (dielectric) frequencies, giving plenty of scope for the eventual experimental observation of the phenomenon with laser pulse trains.

V. Simulation of Birefringence due to Circular Flow

Linear flow induced birefringence[237] is well known and described in the literature. However, appreciating its full potential using molecular dynamics as opposed to hydrodynamics is a more difficult task, and this is true in general of the borderline between flow and molecular dynamics. Recently, however, rapid progress has been made towards the unification of both subjects using computer simulation. Many of the flow phenomena of textbooks in hydrodynamics can now be reproduced directly from the fundamental Newtonian and Eulerian equations of motion, and computers are already in widespread use in practical testing procedures involving flow, over aircraft wings, ships' hulls, and so forth. This illustrates how quickly the seemingly abstract approach can be put to work.

Recent simulations[173] using up to 200,000 atoms over many millions of time steps, have shown how the hydrodynamic properties of a liquid flowing past an object (a disk or a cylinder) can be constructed from Newton's equations of motion. Simulation can reproduce the classical phenomena of hydrodynamics.

Having achieved this agreement between the two branches of physics simulation can confidently advance to the point where new flow phenomena can be anticipated numerically. An example of these is vortex induced birefringence.

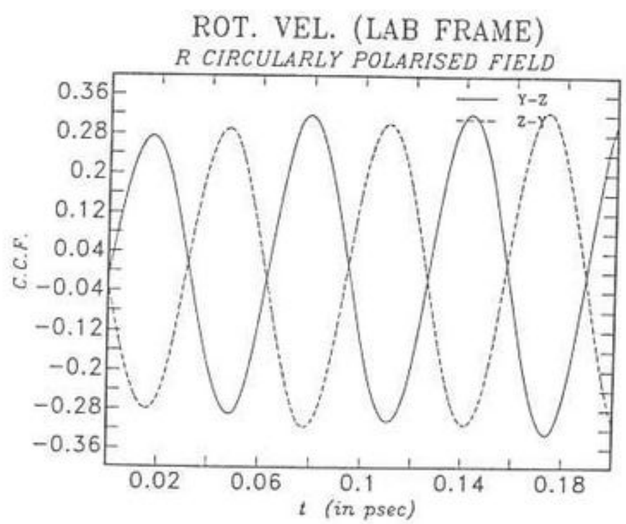

Figure 24. As for Fig. 20, rotational velocity acf.

W. Field Equations for Circular Flow

Circular flow can be induced in a sample of, for example, 500 water molecules in a simulation cell using the simple equations

$$\mathbf{F} = F_Y\mathbf{j} - F_X\mathbf{i} \tag{169}$$

$$F_X = F_0 Y/(X^2 + Y^2)^{1/2} \tag{170}$$

$$F_Y = F_0 X/(X^2 + Y^2)^{1/2} \tag{171}$$

The X and Y components of the flow field are proportional in each case to the radius vector of each molecule's center of mass and propels all the molecules to which it is applied on a vortex about the Z axis. In order to minimise the effect of periodic boundary conditions on the vortex, Eqs. (170) and (171) are set up in an inner cell insulated from the edges at which the boundary conditions apply. At the edges of this inner cell there are natural boundary conditions, individual flowing water molecules encounter those to which no force field has been applied. The molecules in the outer cell shield the vortex from artificial periodicity which would destroy its development over time. Eventually, the flow set up in the inner cell propagates to the outer, forming the beginnings of macroscopic flow. However this occurs very slowly, over millions of time steps, as the applied force field takes effect like a stirring rod.

On a microscopic scale, however, over picoseconds and angstroms, the cell of 500 water molecules may be used to demonstrate numerically the presence of many new patterns of dynamical correlation at the molecular level itself. An example is anisotropy in the correlation tensor of molecular

linear velocity and related dynamical quantities affected by the applied vortex field. The familiar patterns of macroscopic flow, eddies, wakes,a and macroscopic vortices, are always accompanied on the molecular scale by new time cross-correlations at the molecular level. These generate the visible macroscopic phenomena direct from the basic equations of motion, making unnecessary much of the intermediate level of approximation inherent in the subject of hydrodynamics. An example of a measurable effect is vortex induced birefringence.[237] It would be impossible to describe this adequately without the simultaneous consideration of translation and rotation in the diffusing asymmetric top, bringing into consideration both the positional and velocity space, and needing a complicated and insoluble Kramers equation in the approach of Chapter 1. A vortex is made up of many molecules rotating with a definite symmetry in the laboratory frame (X, Y, Z). The theory of Brownian motion in contrast as applied to "purely" rotational or translational diffusion dispenses with adequate consideration of the role of the position vector of center of mass. In rotational diffusion theory there is no consideration of translation and vice versa. To interrelate molecular and flow dynamics it is necessary to identify and define flow fields on a molecular scale. Some preliminary attempts in this direction are described in Refs. 238 and 239.

X. Anisotropy in Linear Diffusion Produced by a Circularly Polarized Laser

This is another new effect[240] and general characteristic of the molecular liquid state discovered by computer simulation. It is also accompanied by a birefringence in the dielectric loss and far infrared power absorption. The effect needs an explanation in terms of the statistical correlation between molecular rotation and translation, exemplified by that between the angular and linear molecular velocities.

Y. Electric or Circularly Polarized Laser Field Applied to a Dilute Gas

We recall from Chapter 1 that the classical-time acf of linear velocity in the infinitely dilute gas is a constant, which can be normalized to one at the arbitrary $t = 0$,

$$\frac{\langle \mathbf{v}(t) \cdot \mathbf{v}(0) \rangle}{\langle v^2(0) \rangle} = 1 \tag{172}$$

On the other hand the equivalent rotational acf of the infinitely dilute gas is[1]

$$\frac{\langle \boldsymbol{\omega}(t) \cdot \boldsymbol{\omega}(0) \rangle}{\langle \omega^2(0) \rangle} = \exp\left(\frac{-kTt^2}{2I}\right) \tag{173}$$

for the spherical top with slightly more complicated expressions for the symmetric and asymmetric top.

If we now consider the imposition of a torque between the dipole moment and the electric field, then the only direct effect is to add a rotational acceleration to each molecule. If there were no molecular interactions, the linear velocities would be unaffected. The linear velocity acf of the dilute gas would remain a constant in time, unaffected by the adjustment to the angular molecular dynamics, and there would be no statistical cross correlation between molecular linear and angular velocities in any frame of reference. We conclude therefore that without the intermediacy of intermolecular interaction there is no way of explaining why a rotational torque generated by an electric field or electromagnetic field through the term $-\boldsymbol{\mu} \times \mathbf{E}$ should result in anisotropy of the center of mass linear velocity acf as illustrated in Fig. 20. The electric or laser field induced linear anisotropy shows, in fact, that in a molecular liquid (as opposed to the infinitely dilute gas) there is always cross correlation between rotational and translational diffusion on the fundamental single molecule level. It is impossible to induce linear anisotropy of the center of mass molecular velocity in the infinitely dilute gas because in this case, and only in this case, the ccf vanishes. In corollary the field induced linear anisotropy of Fig. 20 is a potential experimental method of investigating qualitatively, and perhaps quantitatively, this type of fundamental cross-correlation.

Z. Correlation between Rotation and Translation Induced by Electric Fields

The above argument is supported conclusively by a molecular dynamics computer simulation of the fundamental ccf:

$$\mathbf{C}_3^{ij}(t)_{XYZ} = \frac{\langle \mathbf{v}_i(t)\boldsymbol{\omega}_j(0) \rangle}{\langle v_i^2 \rangle^{1/2} \langle \omega_j^2 \rangle^{1/2}} \tag{174}$$

in the laboratory frame of reference (X, Y, Z) carried out in liquid dichloromethane.[141,142] This result is outside the scope of a purely rotational or translational diffusion theory and therefore of the "up-graded" equation (Eq. 161).

The electric field induces a simple type of ccf directly in frame (X, Y, Z). If the electric field is in the Z axis of the frame (X, Y, Z) it induces the (X, Y) and (Y, X) components of the ccf tensor (Eq. 174), which are equal and opposite. This result can only be described analytically by trying to link together Langevin equations for rotational and translational motion with cross friction coefficients, introducing in the process a

plethora of empiricism. The simple static electric field induces anisotropy according to the Kerr effect, anisotropy which is accompanied by the appearance of a new ccf which is inaccessible to the approach of Section I. The conventional theory of the Kerr effect[9] takes no account of the existence, let alone the detailed time dependence, of this ccf. We must try to adapt the theory to meet the unequivocal indications obtained by computer simulation.

AA. Consequences to the Theory of Polarization

The challenge is however very difficult to meet without introducing too much empiricism, too many unknowns. We have met this problem already in the itinerant oscillator approach and in approximants of the continued fractions of Section I. The existence of a set of nonvanishing ccf's strikes at the very foundations of the theory of diffusion and polarization[9]. The challenge is made with the basic equations of classical dynamics. Also at risk is the conventional approach to fluctuation–dissipation which relates field-on to field-off dynamics. The unaccountable existence of new ccf's which appear when an electric field is switched on and disappear again when it is switched off is not compatible with simply equating an orientation transient to an equilibrium acf. Both the rise and fall transients must reflect the fact that new ccf's are transiently appearing or disappearing as the case may be. The fundamentals of the customary approach to dielectric relaxation take no account of cross correlations whatsoever, and continue to rely on the Debye equation (Eq. 145) in many contemporary treatments. The field-on solution of this equation is a fundamentally inadequate description of the complete process of diffusion in molecular liquids irrespective of the strength of the applied electric field and of the linearity or otherwise of the sample response.

The validity of the Green–Kubo relations linking the translational velocity acf to the translational diffusion coefficient and the rotational and angular velocity acf's to distinctly different, rotational type, coefficients of diffusion, is brought into question whenever a molecular liquid is polarized. The induced ccf's mean that it is doubtful whether purely rotational or purely translational diffusion coefficients ever have an independent existence.

Similarly, a laser can induce first- and higher-order types of birefringence and can polarize the liquid in the same way as an electric field. In this case again we must reckon with the induction of fundamentally new types of cross correlation which accompany the appearance of birefringence and polarization. These ccf's will again be present with flow induced birefringence. These conclusions are made on the basis of the (X, Y) and (Y, X) components of the tensor (Eq. 174) induced by a simple electric

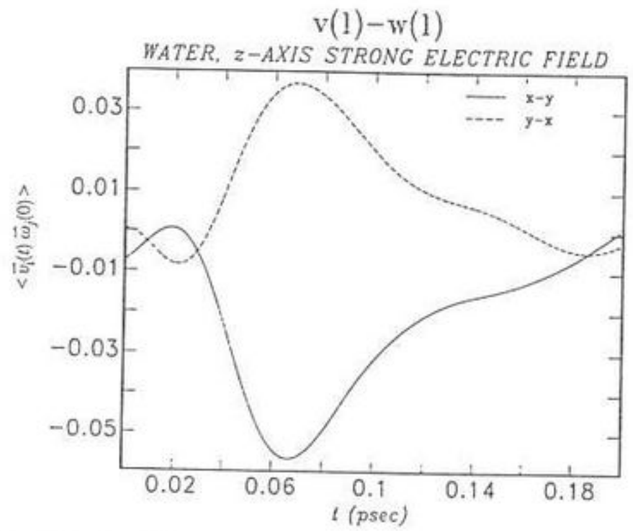

Figure 25. The (X, Y) and (Y, X) elements of the tensor time-correlation function $\mathbf{C}_3^{ij}$ in a Z-axis electric field.

field and illustrated in Fig. 25. The strength of cross correlation, and its time dependence, depend on the electric field strength and also on thc model used of the effective pair potential. The molecular symmetry determines the cross correlation in the molecule fixed frame (x, y, z). As the electric field strength is increased, the ccf's become more oscillatory and show a decoupling effect. The ccf vanishes at $t = 0$ and $t \to \infty$. With accurate enough computer simulations it is probable that the ccf's would show long time tails which are difficult to observe because of their low amplitude.

BB. Diffusion Equations for Rotation and Translation

The analytical description of the molecular liquid state needs diffusion equations which are capable of describing the simultaneous rotation and translation of the diffusing molecule in three dimensions. Progress may be attempted either by extending and modifying the old theory or by depending more and more on computer simulation while checking the latter with actual experimental data. Section V deals in greater detail with the attempts made in the last few years to extend the boundary of validity of molecular diffusion, and in this closing part of Section IV we describe and attempt to define the problems associated with this analytical extension.

1. *The Problem of Analytical Tractability*

We have encountered a recurring and increasingly severe general constraint on the traditional theoretical approach to molecular diffusion, that of complexity and mathematical intractability. Within the strictly defined and somewhat artificial limits of rotational diffusion theory the problem is kept under control by ad hoc assumptions about the nature of the intermolecular potential and of the rotational mechanics of a rotating molecule. In this context the rotational diffusion theory has not progressed much beyond the theory of the nonlinear itinerant oscillator, which effectively reduces the rotational problem to two dimensions and uses a very simple approximation to the intermolecular potential. Even then, the Langevin equations (Eqs. 36 and 37) are insoluble directly, and must be put into the form of a Kramers equation which can only be solved numerically,[41,42] frequently consuming as much computer resource as a full computer simulation.

As we have seen in Section I these equations are analytically fully equivalent to an early approximant of the Mori continued fraction, and this fixes their relation to the Liouville equation. The itinerant oscillator equations contain a number of parameters, friction coefficients, moments of inertia, and harmonic force constants, which can only be guessed at, making the description empirical. A historical perspective reveals clearly that the analytical approach has been slow to evolve, and has frequently failed to anticipate new effects discovered numerically or experimentally. The rotational diffusion equation resulted in the physically meaningless Debye plateau and the translational equation missed the existence of long time tails and negative regions in the velocity acf. The theory is now faced with the emergence of a set of new ccf's.

2. *The Problem of Over-Parameterization*

The simplest type of ccf requires for its description a linked Langevin structure such as[141,142]

$$m\dot{\mathbf{v}} + \beta_v \mathbf{v} + \beta_{v\omega}\boldsymbol{\omega} = \mathbf{F} \tag{175}$$

$$I\dot{\boldsymbol{\omega}} + \beta_\omega \boldsymbol{\omega} + \beta_{\omega v}\mathbf{v} + E_0 \sin \Theta t = \mathbf{Tq} \tag{176}$$

Here $\mathbf{v}$ is the molecular center-of-mass linear velocity, $\boldsymbol{\omega}$ the angular velocity of the same molecule, m the molecular mass, I an "effective" moment of inertia, β_v the translational friction coefficient, β_ω the rotational friction coefficient, and $\beta_{v\omega}$ and $\beta_{\omega v}$ are cross friction coefficients designed to link the two types of motion purely empirically. $\mathbf{F}$ is a stochastic force and $\mathbf{Tq}$ a stochastic torque. The field term $E_0 \sin \Theta t$ is needed to represent the interaction between the external electric field and molecular dipole, to polarize the liquid for observation by dielectric spectroscopy and to make the sample birefringent for Kerr effect observation. It also induces the existence of new ccf's. To approximate this complicated pair of nonlinear stochastic differential equations would lead back to separated rotational and translational diffusion, thus defeating the purpose of the exercise. In this decoupled form the theory is able to force fit some of the least discriminating of data, such as low frequency dielectric loss, but gets no further below the surface.

A more difficult but necessary approach would be to attempt the direct solution of Eqs. (175) and (176) simultaneously.[141,142] The solution contains four friction coefficients which cannot be expressed in terms of the fundamental physical constants. Given four independent data sources, the four could be found in principle, but in practice this has never been attempted. Such a combination might involve, for example, far infrared spectra, dielectric spectra, Rayleigh scattering data, and various forms of NMR data. These sources would have to be wide ranging and discriminating. Assuming for the sake of argument the availability of such data we would determine four friction coefficients. What would we have achieved?

We would have arrived at four numbers with which to characterize the molecular diffusion process. However, we know independently that the equations upon which these numbers are based are approximate and imperfect descriptions of the molecular dynamical process. The friction coefficients are first approximations to time dependent memory functions, a hierarchy of which is needed to build up the Liouville equation. The equations contain no acceptable description of what is known from quantum mechanics to be the accurate form the pair potential must take. The Langevin equations (Eqs. 175 and 176) would not be able to provide an explanation of effects such as fall transient acceleration and field decoupling. Knowing all this, it would be useless to pretend that our four numbers would be anything more than the parameters of a curve-fiitting exercise.

An additional constraint is that Eqs. (175) and (176) become insoluble without the use of an effective moment of inertia I which approximates the kinematics of an asymmetric top with those of a spherical top. More rigorous consideration leads back to the Euler–Langevin equations (Eqs. 68 to 70) which are analytically insoluble even when no account of translation is made, and which introduce yet more friction coefficients.

The next section attempts to describe how molecular dynamics can be tackled with a combination of group theory and computer simulation. We have arrived at a point where the traditional methodology of natural philosophy, observation followed by description and hypothesis, followed by a repetition of the cyclical gathering of understanding, has been modi-

fied to involve consideration of many data sources interpreted with computer simulation. The course of this advance is made smoother with the symmetry principles of the next section.

V. SYMMETRY

The diffusion of a rigid asymmetric top occurs in three dimensions and involves simultaneous rotation and translation. We have seen in Sections I–IV that the available theories of molecular diffusion cannot describe this process adequately because of intractability and empiricism. An experimental understanding needs data from as many sources as possible interpreted with computer simulation. Without theory or data, however, considerable insight may be obtained from considerations of symmetry. These include the fundamental symmetry operations of classical physics, such as parity inversion and time reversal, and the rules of point group theory. Symmetry considerations alone can be used to determine the existence or otherwise of statistical correlation in an ensemble of diffusing asymmetric tops, and they can be applied in the frame (X, Y, Z) of the laboratory or (x, y, z) fixed in the molecule. The symmetry rules to be developed in this chapter and in Sections VII and VIII should be used before starting to simulate the properties of the ensemble. They filter out the ccf's that vanish for all t from those that may exist and which therefore may be detected numerically. They do not provide the detailed time dependence of any correlation function or frequency dependence of any spectrum, these have to be found from equations of motion.

An example of a symmetry rule at work is the use of parity reversal to show that the ccf

$$\mathbf{C}_3^{ij}(t)_{XYZ} = \frac{\langle \mathbf{v}_i(t)\boldsymbol{\omega}_j(0)\rangle}{\langle \nu_i^2\rangle^{1/2}\langle \omega_j^2\rangle^{1/2}} \tag{177}$$

must vanish for all t because the parity symmetry of $\mathbf{v}$ is negative and that of $\boldsymbol{\omega}$ is positive. However the same is not true in frame (x, y, z) and here certain elements of the tensor

$$\mathbf{C}_3^{ij}(t)_{xyz} = \frac{\langle \mathbf{v}_i(t)\boldsymbol{\omega}_j(0)\rangle}{\langle \nu_i^2\rangle^{1/2}\langle \omega_j^2\rangle^{1/2}} \tag{178}$$

exists for $t > 0$, a result first discovered[47] by computer simulation. Again the traditional theory of diffusion failed to predict or anticipate the result.

There are available several fundamental symmetry operations, which should be applied in order of applicability. The most generally valid operation should be applied first, and the less general thereafter. What follows is a brief summary of the most useful symmetry operations.

A. Parity Inversion

The parity inversion operation in frame (X, Y, Z) is defined as

$$\hat{P}: (\mathbf{p}, \mathbf{q}) \rightarrow (-\mathbf{p}, -\mathbf{q}) \tag{179}$$

where $\mathbf{p}$ is the molecular momentum and $\mathbf{q}$ its position. It inverts all positions and momenta, so that, for example $(X, Y, Z) \rightarrow (-X, -Y, -Z)$. The linear velocity is therefore negative to parity inversion but the angular velocity is an axial vector defined by the vector cross product between linear velocity and position, two quantities which are negative to parity reversal. In consequence the angular velocity is positive to parity reversal. Similarly the linear acceleration $\dot{\mathbf{v}}$ is negative to this operation and the angular acceleration positive. None of these considerations apply in the molecule fixed frame (x, y, z)

B. Time Reversal

The time-reversal symmetry rule is

$$\hat{T}: (\mathbf{p}, \mathbf{q}) \rightarrow (-\mathbf{p}, \mathbf{q}) \tag{180}$$

and reverses the sign of time dependent quantities in frame (X, Y, Z). Linear and angular velocity depend on time and are reversed by the operation (Eq. 180). Both are negative to time reversal. The linear and angular accelerations, however, are both positive to time reversal and this may be seen by considering them as velocity divided by time. The latter is given a negative label by time reversal, and accelerations in terms of operation (Eq. 180) are negative quantities divided by negative, being therefore overall positive to time reversal.

C. Application to Time-Correlation Functions

In an isotropic ensemble of molecules at reversible thermodynamic equilibrium, the ensemble average $\langle \mathbf{ABC} \ldots \rangle$ may exist in frame (X, Y, Z) if the product $\hat{P}(\mathbf{A})\hat{P}(\mathbf{B})\hat{P}(\mathbf{C}) \ldots$ is positive. If this product is negative the ensemble average vanishes. If the ensemble average is a time correlation function, the latter vanishes for all t if the product is negative.

This is the most generally applicable rule, and a simple proof is given in Ref. 241.

Note that if the molecular liquid is not isotropic or if the Hamiltonian itself becomes negative to parity inversion, the rule may no longer be applied as it stands, and we must refer to the three principles of group theoretical statistical mechanics developed in Chapter 7.

If the product is positive the ensemble average is subjected to the next test, which is time reversal. This operation must be applied with great care, because it can be misleading when applied to correlation functions. For example, thc acf's $\langle \mathbf{A}(t) \cdot \mathbf{A}(0) \rangle$ or $\langle \mathbf{B}(t) \cdot \mathbf{B}(0) \rangle$ are always positive to time reversal, and the operation does not change the value of the correlation function at $t = 0$ from positive to negative. However, for some ccf's such as $\langle \mathbf{A}(t) \cdot \dot{\mathbf{A}}(0) \rangle$ or $\langle \mathbf{B}(t) \cdot \dot{\mathbf{B}}(0) \rangle$ time reversal also reverses the sign of the correlation function at $t = 0$ from positive to negative. In this case the time reversal rule does not apply, and nothing more can be said about the time existence or otherwise of the cross correlation function. Therefore, the time reversal rule is applicable in general to ccf's which are known by inspection to have a zero slope at the time origin $t = 0$. It is therefore less general in nature than parity reversal symmetry.

D. The Application of Group Theory to Time Correlation Functions

If an ensemble average has passed the tests of parity and time reversal, point group theory may be applied in the frames (X, Y, Z) and (x, y, z). However, in frame (X, Y, Z) the symmetry rules must be applied in the correct order: (1) parity inversion, (2) time reversal, (3) point-group theory. For example, point group theory allows the existence of the cross correlation function $\mathbf{C}_3^{ij}$ frame (X, Y, Z) for some ensembles of chiral molecules, but parity reversal considerations do not. Therefore the ccf must vanish in frame (X, Y, Z) for all t for both enantiomers and the racemic mixture. In frame (x, y, z) point group theory may be used to pinpoint the existence of ensemble averages with reference to *the molecular point group character tables*. Dichloromethane, for example, has C_{2v} molecular point group symmetry, allowing two off-diagonal elements of $\mathbf{C}_3^{ij}$ to exist in frame (x, y, z). These are independent elements with different time evolutions, obtainable[1–4] from computer simulation. The signature of cross correlation between linear and angular velocities is obtained in frame (x, y, z) but vanishes in (X, Y, Z).

E. Point-Group Theory in Frame (X, Y, Z)

Point group theory is a well-developed subject which has recently been applied to ensemble molecular dynamics by Whiffen[242] and the present author, (Sections VII and VIII). The basic assumption in the application of group theory to ensemble molecular dynamics in frame (X, Y, Z) is embodied in the first principle of group theoretical statistical mechanics developed in Section VII. If the point group symmetry representation of the dynamical variable $\mathbf{A}$ is denoted $\Gamma(\mathbf{A})$, then the symmetry representation of the ensemble average $\langle \mathbf{A} \rangle$ is assumed to be the same as that of $\mathbf{A}$. If the representation $\Gamma(\langle \mathbf{A} \rangle)$ contains the totally symmetric representation

of the point group of frame (X, Y, Z), then the ensemble average may exist, subject to passing the tests of parity inversion and time reversal.

The theory can be applied to scalars, pseudoscalars, polar and axial vectors, and tensors representing molecular dynamical quantities of interest. Polar vectors such as linear velocity are negative to parity inversion, whereas axial vectors such as angular velocity are positive. Scalars are always positive to both time $\hat{P}$ and $\hat{T}$, and pseudoscalars such as the optical activity coefficient reverse sign between enantiomorphs. A molecular dipole moment and electric field are both polar vectors, while a magnetic dipole moment and a magnetic field are axial.

Molecular polarizability and moment of inertia tensors are second order cartesian quantities. Third order cartesian tensors have $3 \times 3 \times 3 = 27$ elements and so on. Here n is used for the order of the tensor and n_s denotes the number of suffix pairs in which the tensor is symmetrical. If this is nonzero, the number of independent elements, denoted n_i, is less than the number of elements.

If any quantity is positive to $\hat{P}$, it is labelled by the suffix g. If negative it is labelled u. These come from the spectroscopic terms "gerade" or "ungerade".

The friction tensor (whose elements are Langevin friction coefficients), and the molecular moment of inertia tensor are each 3×3 tensors with $n_s = 1$ and $n_i = 6$.

Time correlation functions in this context are valid tensor elements to which symmetry theory can be applied both in frames (X, Y, Z) and (x, y, z). The tensor is usually a 3×3 Cartesian whose elements are individual ccf's. Point group theory can say nothing about the actual time dependence of these elements, but is used to indicate whether or not they vanish by symmetry in frames (X, Y, Z) and (x, y, z). The time dependence of existing elements may be different for the same type of correlation in different frames, and will be nonzero only if they contain the fully symmetric representation of the point group.

The point group of frame (X, Y, Z) is the rotation–reflection group $R_h(3)$ and the symmetries of quantities in this frame are denoted through the irreducible D representations with subscript g or u and superscripts $0, 1, 2, \ldots$ In this notation the scalar quantity is $D_g^{(1)}$, the pseudoscalar is $D_u^{(0)}$, the polar vector is $D_u^{(1)}$, the axial vector is $D_g^{(1)}$; and higher order tensors are subscripted g or u and superscripted $2, 3, 4, \ldots$ This notation is used extensively in Sections VII and VIII.

The product of two or more D representations can be built up with the help of the Clebsch–Gordan Theorem, which can be expressed in the form

$$D^{(n)} D^{(m)} = D^{(n+m)} + \cdots + D^{|(n-m)|} \tag{181}$$

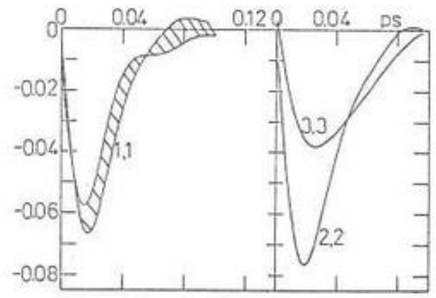

Figure 26. The third-rank tensor $\langle \mathbf{v}(t) \times \omega(t) \mathbf{v}^T(0) \rangle_{xyz}$ for liquid water.

The rule for the product of subscripts is $g \times g = g$; $u \times u = g$; $g \times u = u \times g = u$. If we are looking at the correlation function of a product of linear and angular velocities, the symmetry representation of the correlation function is in general the product of $D_u^{(1)}$ and $D_g^{(1)}$. Equation (181) shows this to be a sum of three parts. All three are however, negative to parity reversal, because each carries the subscript u. This type of ccf does not survive the test of parity inversion, which is more general than group theory, and it vanishes in frame (X, Y, Z). Similarly, the triple ccf $\langle \mathbf{v}(t) \times \boldsymbol{\omega}(t) \cdot \mathbf{v}(0) \rangle$ vanishes in frame $(X, ,Y, Z)$. In frame (x, y, z), however, independent elements exist, and one of these is illustrated in Fig. (26) from a recent computer simulation.[243]

F. Frame (x, y, z), Molecular Point-Group Theory

The point group for the molecule fixed frame is that of the individual molecule.[244] In order to make use of point group theory in this frame the irreducible representations of each quantity have to be mapped from frame ,(X, Y, Z). The existence of an ensemble average in frame (x, y, z) is then determined by the principles of group theoretical statistical mechanics, developed in Section VII. Morc details of the mapping procedures are given in that Section.

G. Ensemble Averages of Scalars

Quantities such as mass and charge are simple scalars which are invariant to frame transformation. In the language of point group theory, this means that the totally symmetric representation in the point group $R_h(3)$ maps on to its equivalent in any molecular point group. The ensemble average of a scalar quantity always exists in both frames (X, Y, Z).

H. Ensemble Averages of Vectors

No vector contains the totally symmetric representation $D_g^{(0)}$ and the ensemble average of any vector quantity at field free thermodynamic equilibrium vanishes in frame (X, Y, Z). This is not necessarily so in frame

(x, y, z), however, and vector ensemble averages may be observable in this frame if also positive to parity inversion and time reversal.

I. Ensemble Average of Tensors

Some tensor quantities such as molecular polarizability contain the totally symmetric representation of $R_h(3)$ at least once. Ensemble averages over these quantities therefore exist in frame (X, Y, Z). Examples are the traces (isotropic diagonal parts) of the molecular polarizability and magnetizability, and moments of inertia. The D representation of a tensor quantity may be mapped from frame (X, Y, Z) to (x, y, z), and the number of independent ensemble averages over tensor elements in each frame may be different. This argument is developed in more detail in Section VII. In general, there may be more independent ensemble averages in frame (x, y, z) than in frame (X, Y, Z), depending on the symmetry of the molecule.

J. Ensemble Average Properties in Frame (x, y, z)—Some Examples

In the C_{2v} point group of dichloromethane, for example, there may be three independent averages of a vector quantity which is positive to parity inversion and time reversal. There are none in frame (X, Y, Z). For a symmetric top of C_{3v} symmetry such as chloroform, two of these averages in frame (x, y, z) are equal and different from the third. In a spherical top such as carbon tetrachloride all three averages in frame (x, y, z) are equal. For all molecular symmetries they vanish in frame (X, Y, Z).

The cross-correlation function between molecular linear and angular velocity is in general a 3×3 tensor, all of whose elements vanish in frame (X, Y, Z) at isotropic reversible equilibrium. In frame (x, y, z) this is not necessarily so. For the molecular point group symmetries C_{2h}, C_{2v}, C_{3v}, and T_d, for example, there are $0, 2, 1, 0$ nonzero elements of this ccf respectively. A C_{2v} asymmetric top such as dichloromethane or water has two independent elements of the ccf in its frame (x, y, z) which can be found using the point group character tables as described in (242). These were originally discovered by computer simulation[3,4] and are illustrated in Fig. 27. The elements found by simulation exactly match those confirmed [242] by group theory. Both simulation and symmetry continually pose new challenges to the original theoretical approach (Chapter 1).

A molecule of C_{3V} symmetry only has one independent element of the ccf tensor, and this is again what is found by simulation.[196] However, for molecules of C_{2h} and spherical top symmetry all elements of the ccf vanish in frame (x, y, z). The point group theory applies to all known molecular

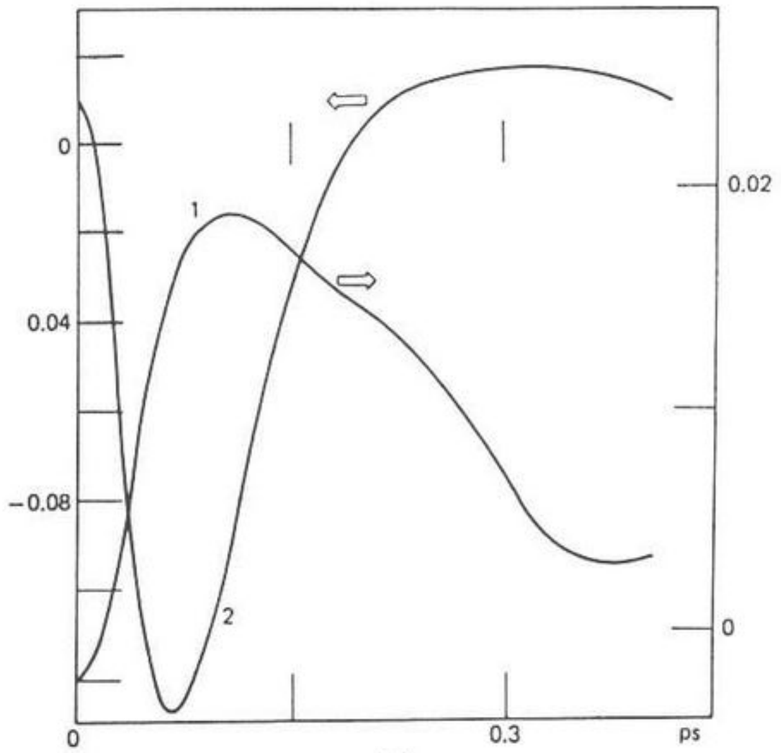

Figure 27. Nonvanishing off-diagonal elements of the second-rank tensor $\langle \mathbf{v}(t)\omega^T(0)\rangle_{xyz}$ for liquid dichloromethane.

symmetries, and is confirmed by available computer simulation results.[47] In chiral molecules all nine elements of thc ccf matrix may exist, and all change sign from one enantiomorph to the other and vanish in the racemic mixture.

K. Higher Order Tensors

There are many rank three tensors which characterize simultaneous rotation and translation through the appropriate time ccf's. None of these is yet available in diffusion theory, but both group theory and computer simulation show their existence in frames (X, Y, Z) and (x, y, z). In this case the group theory allows many independent elements, whose identity can be found by detailed reference to the point group character table. In the laboratory frame, however, they must be positive to parity inversion in order to have a time dependence for $\tau > 0$, and if they pass this test, they play a role in the intercorrelation of rotation and translation. An illustration[243] is given in Fig. 28. In physical terms the existence of a time ccf such as this means[242] that the Coriolis acceleration $2\mathbf{v} \times \boldsymbol{\omega}$ plays a direct role in mixing rotational and translational velocities. This is the acceleration which stops a spinning and precessing top from falling over

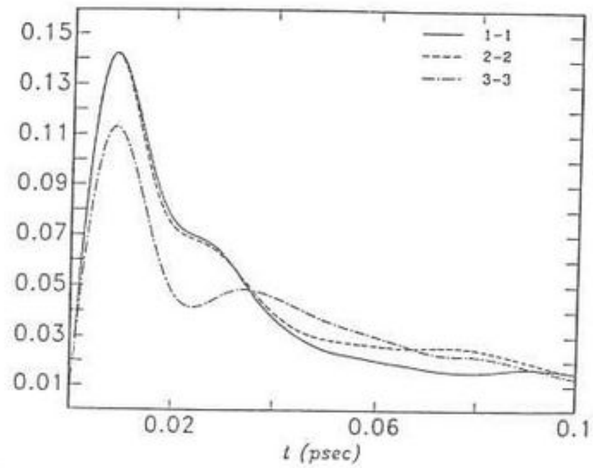

Figure 28. Illustration from computer simulation of the laboratory frame ccf; $\langle \mathbf{v}(t)\times\omega(t)\dot{\mathbf{v}}(0)\times\omega(0))^T\rangle_{XYZ}$.

because it is in opposition to gravity. Point group theory allows, for instance, a statistical correlation to exist in frame (X, Y, Z) between the Coriolis acceleration of a molecule at time t and its own linear acceleration a time t earlier for all molecular symmetries, including the spherical top. It is illustrated for carbon tetrachloride[57] in Fig. 28.

For a molecule of C_{2v} symmetry such as dichloromethane, point group theory allows the possible existence of a g-type ccf such as $\mathbf{C}_4 = \langle \mathbf{v}(t) \times \boldsymbol{\omega}(t) \cdot \mathbf{v}(0)\rangle$ in frame (x, y, z), but this ccf fails the test of time reversal symmetry and vanishes in frame (X, Y, Z) for all t.[203–206] In frame (x, y, z) on the other hand the parity and time reversal rules are not applicable, and point group theory allows the existence of no less than six independent elements. These come from the vector product in the Coriolis acceleration, so that the general symmetry of the ccf is

$$\mathbf{C}_4 = \begin{bmatrix} + & 0 & 0 \\ 0 & + & 0 \\ 0 & 0 & + \end{bmatrix}_{xyz} \tag{182}$$

and the three elements are illustrated in Fig. 29.

For all ranks of ungerade tensors in frame (X, Y, Z) all elements vanish in frame (X, Y, Z). However, in frame (x, y, z), elements may exist depending on the molecular point group symmetry. An example is the general triple product

$$\mathbf{C}_5(t) = \langle \boldsymbol{\omega}(t)\mathbf{v}(t)\boldsymbol{\omega}(0)\rangle \tag{183}$$

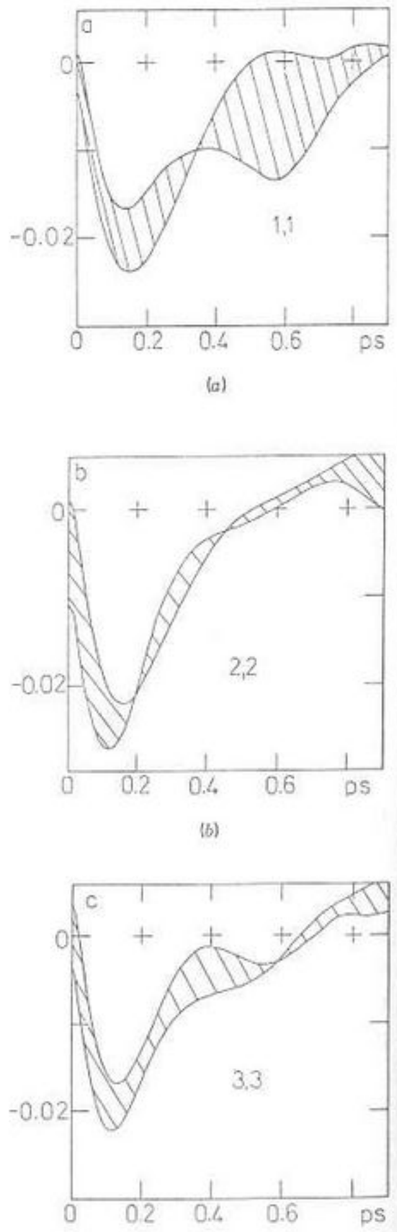

Figure 29. Laboratory frame ccf's for the spherical top carbon tetrachloride in the liquid state, from a recent computer simulation.[57]

in which the several separate elements can be investigated by computer simulation.

In general, in frame (x, y, z), as we increase the point group symmetry from asymmetric to spherical top the number of independent elements decreases, and in this respect computer simulation and point group theory are in detailed agreement. Enantiomorphs containing optically active

molecules of low symmetry tend to have the largest number of nonvanishing elements.

The effect of external fields was introduced in Section IV and different types of fields have different effect according to the third principle of group theoretical statistical mechanics, described in Section VII. The electric field, for example, makes visible extra elements of cross correlation between linear and angular velocities in frame (X, Y, Z), elements which are negative to parity inversion in the absence of the field. The electric field itself is negative to parity inversion, and it imparts this symmetry characteristic to certain ensemble averages.

Normally gravitational fields are small in comparison with electric, magnetic and electromagnetic fields, or mechanical force fields such as those encountered in shear or elongational flow (Section VIII). Any of these fields may remove the symmetry of the sample at equilibrium. The interaction of an electric field with the ensemble may occur through different powers of the electric field strength **E** with the molecular dipole; E^2 with the molecular polarizability; E^3 with the hyperpolarizability, and so on. In the presence of fields, the general rules on parity and time reversal no longer apply, because the Hamiltonian itself has become affected by the external field. In this case the most general rules available are those provided by point group theory in both frames. These are summarized in the third principle of Section VII.

M. Fundamental Dynamics: The Noninertial Frame of Reference

The intricate relation between rotational and translational variables in molecular diffusion becomes clear if we consider a frame transformation[245] from the laboratory frame (X, Y, Z) to a rotating frame $(1, 2, 3)$ whose origin is the same as that of the laboratory frame. A theorem of elementary dynamics [246] links the differential operator $\hat{D}_f$ in frame (X, Y, Z) to its equivalent $(\hat{D}_m)$ in $(1, 2, 3)$. Considering the position vector of the molecular center of mass the theorem is

$$\hat{D}_f \mathbf{r} \equiv (\hat{D}_m + \boldsymbol{\omega} \times)\mathbf{r} \tag{184}$$

and conversely

$$\hat{D}_m \mathbf{r} \equiv (\hat{D}_f - \boldsymbol{\omega} \times)\mathbf{r} \tag{185}$$

The operator $(\hat{D}_m + \boldsymbol{\omega} \times))$ in frame $(1, 2, 3)$ is equivalent to the operator $\hat{D}_f$ in (X, Y, Z), and conversely in Eq. (185). Rewriting these equations in terms of velocities gives